https://doi.org/10.5194/egusphere-2025-1264
Preprint. Discussion started: 28 March 2025

Impact of topography and meteorological forcing on snow simulation in the Canadian Land Surface Scheme Including Biogeochemical Cycles (CLASSIC)

Libo Wang[1], Lawrence Mudryk[1], Joe R. Melton[2], Colleen Mortimer[1], Jason Cole[3], Gesa Meyer[2], Paul Bartlett[1], and Mickaël Lalande[4,5]

1 Climate Processes Section, Climate Research Division, Environment and Climate Change Canada, Toronto, ON, Canada

2 Climate Processes Section, Climate Research Division, Environment and Climate Change Canada, Victoria, BC, Canada

3 Canadian Centre for Climate Modelling and Analysis, Climate Research Division, Environment Canada, Victoria, BC, Canada

4 Centre for Research on Watershed-Aquatic Ecosystem Interactions, Environmental Sciences Department, Université du Québec à Trois-Rivières, Trois-Rivières, QC, Canada

5 Centre for Northern Studies, Université Laval, QC, Canada

Corresponding author: Libo Wang, libo.wang@ec.gc.ca

https://doi.org/10.5194/egusphere-2025-1264
Preprint. Discussion started: 28 March 2025

Abstract

Our study evaluates the impacts of an alternate snow cover fraction (SCF) parameterization on snow simulation in the Canadian Land Surface Scheme Including Biogeochemical Cycles (CLASSIC). Three reanalysis-based meteorological datasets are used to drive the model to account for uncertainties in the forcing data. While the default parameterization assumes a simple linear relationship between SCF and snow depth with no dependence on topography, the alternate parameterization accounts for the topographic effects of sub-grid terrain on SCF. We show that the alternate parameterization improves SCF simulated in CLASSIC during winter and spring in mountainous areas for all three choices of meteorological datasets. Annual mean bias, unbiased root mean squared area, and correlation improve by 75 %, 32 %, and 7 % when evaluated with MODIS SCF observations over the Northern Hemisphere. We also demonstrate that the improvements to simulated SCF lead to further improvements in variables related to surface radiation, energy fluxes, and the water cycle. Finally, we link relative biases in the meteorological forcing data to differences in simulated snow water equivalent and SCF. Assessment of simulations with different combinations of SCF parameterizations and meteorological datasets reveals the large impact of meteorological forcing on snow simulation in CLASSIC. Two out of the three meteorological datasets were bias-adjusted using observation-based datasets. However, simulations forced by the dataset without bias correction outperform relative to simulations forced by datasets with bias correction, suggesting that there are large uncertainties in the observation-based datasets and/or methods used for bias correction. This study underscores the importance of accounting for topographic effects of sub-grid terrain and accurate meteorological forcing on snow simulation in land surface models.

1. Introduction

Snow cover exists from six to nine months of the year at the high latitudes and high elevations of mountainous regions. The seasonal transition from snow covered to snow free conditions can have a large impact on the stability of permafrost, the length of the active growing season, and surface water and energy balances due to the much higher albedo of snow cover than other land surfaces (e.g., Myneni et al., 1997; Betts et al., 1998; Osterkamp and Romanovsky, 1999; Frolking et al., 2006). Snow cover plays an important role in the regional and global climate system because of the snow-albedo feedback mechanism (Fletcher et al., 2009; Qu and Hall, 2013). Any uncertainty in the magnitude of this climate feedback decreases our ability to reduce uncertainty in climate sensitivity (Roe and Baker, 2007). Therefore accurate simulation of snow cover is crucial for future climate predictions in climate and Earth system models (ESMs).

Snow depth (SND) varies at scales from about 10 to 100 m as a result of heterogeneity in land cover, terrain, and meteorological conditions (Liston 2004), while a typical ESM grid cell size is about 100 km or more. Most land surface models (LSMs) explicitly treat only some of this heterogeneity, for example by accounting for different land cover types within a grid cell (Verseghy et al., 2017). Snow cover fraction (SCF) parameterizations are commonly used to account for unresolved (sub-grid scale) snow depth variability. However, most models from the

https://doi.org/10.5194/egusphere-2025-1264
Preprint. Discussion started: 28 March 2025

Coupled Model Intercomparison Project (CMIP) phase 5 (Taylor et al., 2012) and phase 6 (Eyring et al., 2016) have been found to overestimate SCF in mountainous regions, often with a corresponding cold bias in surface air temperature (Su et al., 2013; Lalande et al., 2021). These biases are also present in the most recent Canadian Earth System Models (CanESM5, Swart et al., 2019; Sigmond et al., 2023) and the latest version of its land surface component, the Canadian Land Surface Scheme Including biogeochemical Cycles (CLASSIC, Melton et al., 2020; Seiler et al., 2021). The SCF overestimation has been attributed to many potential causes, such as too much precipitation and/or overly simplistic SCF parameterizations in ESMs (Lalande et al., 2021; Miao et al., 2022).

Most SCF parameterizations in LSMs estimate SCF based on its relationship with SND or snow water equivalent (SWE) (e.g., Marshall and Oglesby,1994; Douville et al., 1995; Yang et al., 1997; Roesch et al., 2001; Niu and Yang, 2007; Swenson and Lawrence, 2012; Lalande et al., 2023). Some of these parameterizations also account for topographic effects of sub-grid terrain on SCF (e.g., Douville et al., 1995; Roesch et al., 2001; Swenson and Lawrence, 2012; Lalande et al., 2023), which have been demonstrated to be crucial in mountainous regions (Miao et al., 2022). In CLASSIC, the default parameterization historically used is a linear relationship between SCF and SND with no dependence on topography. A grid cell is considered fully snow-covered when the diagnosed SND reaches 0.1 m. Melton et al. (2019) investigated the impact of two alternative SCF parameterizations on SCF and permafrost area simulated by CLASSIC. The first was to change the SCF-SND linear relationship to a hyperbolic tangent function (Yang et al., 1997), and the second was to change the SCF-SND linear form to an exponential form (Brown et al., 2003). Both alternative SCF parameterizations worsened performance in terms of the global permafrost area and active layer thickness, neither was implemented.

Here we consider another option previously developed by Swenson and Lawrence (2012). Their parameterization (hereafter referred as SL12) qualitatively reproduces the hysteresis present in the observational data (SCF-SND relationship) between snow accumulation and ablation seasons while also accounting for the topographic effects of sub-grid terrain. The SL12 parameterization was implemented in the Community Land Model version 5 (CLM5), the land surface component in the Community Earth System Model version 2 (CESM2). Notably, CESM2 was one of the models that showed the lowest surface air temperature and SCF biases over the High Mountainous Asia (HMA) region among the CMIP6 models (Lalande et al., 2021). Based on these results, the SL12 parameterization was implemented in the CLASSIC model and here we evaluate the impact of this change on SCF, SWE, and other snow-related land surface variables. Our evaluation is based on offline CLASSIC simulations forced by historical temperature and precipitation from reanalyses. Because there is uncertainty in these historical values, especially in mountainous regions, we use three different reanalysis-based meteorological datasets to drive CLASSIC. For each meteorological forcing datasets we perform two CLASSIC simulations, one with the default SCF parameterization and one with the SL12 parameterization. The two parameterization schemes are compared with observed SCF and SWE, and the other snow-related land surface variables are evaluated using the Automated Model Benchmarking R package (AMBER, Seiler et al., 2021). The remainder of this paper is organized as follows. In Section 2, we describe the CLASSIC model, the two SCF parameterizations, the forcing data,

https://doi.org/10.5194/egusphere-2025-1264
Preprint. Discussion started: 28 March 2025

and model setup. In Section 3, we describe the observation data and our evaluation methods. Results are detailed in Section 4 and discussion points in Section 5. We present conclusions in Section 6.

2. CLASSIC model, SCF parameterization methods, and model setup

2.1 CLASSIC description and snow model characteristics

CLASSIC is an open-source community land model that is designed to address research questions that explore the role of the land surface in the climate system. It is the successor to the coupled modelling framework based on the Canadian Land Surface Scheme (CLASS; Verseghy, 1991; 1993) and the Canadian Terrestrial Ecosystem Model (CTEM; Arora and Boer, 2005; Melton and Arora, 2016). The physics and biogeochemistry modules of CLASSIC are based on CLASS and CTEM models, respectively. Older versions of CLASSIC (under the name CLASS-CTEM) have served as the land component in the family of Canadian Earth System Models (CanESM) which contribute to the CMIPs (Swart et al., 2019).

The physics component of CLASSIC models energy and water balances separately for the vegetation canopy, snow, and soil (Verseghy, 1991; Melton et al., 2019). As a first-order treatment of subgrid-scale heterogeneity, each grid cell is divided into four sub-areas, consisting of vegetated and bare soil areas, each with and without snow cover. Snow is represented as single layer, which includes canopy snow processes such as interception, unloading, sublimation and melt (Bartlett et al., 2006; Verseghy et al., 2017). The grid cell albedo is computed as a weighted mean based on the fractional coverages for each surface type. In previous versions of CLASSIC, the snow albedo decreases exponentially with time from fresh snow values according to empirically derived functions (Verseghy, 1991). In more recent versions, a new physics-based snow albedo parameterization is available, which accounts for contributions of black carbon snow mixing ratio and the effective snow grain size on snow albedo (Namazi et al., 2015). The new snow albedo scheme is the default scheme in CanESM models and is used in this study. Further details on the CLASSIC model can be found in Melton et al. (2020).

2.2 SCF parameterization methods

2.2.1 The current default SCF parameterization

In CLASSIC, the thicknesses of all vertical layers are recommended to be greater than 0.1 m to avoid numerical instability problems. Therefore, the local SND over the snow-covered portion of a grid cell is not allowed to decrease below this threshold (0.1 m), instead, the fractional snow cover decreases to conserve snow mass. Snow cover is considered complete when SND reaches 0.1 m; when SND < 0.1 m, SCF is computed as SCF = SND/0.1, and SND is reset to 0.1 m. Hereafter we refer to the current default SCF parameterization as the Control (CTL) parameterization. Previous analysis has shown that increasing or decreasing this threshold value by 50 % has little effect on the simulated SWE or SCF (Verseghy et al., 2017).

https://doi.org/10.5194/egusphere-2025-1264
Preprint. Discussion started: 28 March 2025

2.2.2 The SL12 SCF parameterization

Based on snow cover datasets at relatively high spatial and temporal resolution, Swenson and Lawrence (2012) demonstrated that the relationship between SCF and SND depends not only on the amount of snow, but also on month of the year. This dependence is hypothesized to stem from differences in how accumulation versus ablation processes alter the correlation of the two variables. Based on this they proposed separate formulations for snow accumulation and melt periods as follows.

During snow accumulation:

$$f_{sno}^{n} = 1 - ((1 - \tanh(k_{acc}\Delta W))(1 - f_{sno}^{n-1}) \quad (1)$$

Where f_{sno}^{n} and f_{sno}^{n-1} are SCF from the current and the previous time step, k_{acc} is a scale parameter (mm^{-1}) and ΔW (mm) is the amount of new snow that falls within the current time step. Note Eq. (1) is the formulation used in CLM5 code (and implemented in CLASSIC), which is different from that in Swenson and Lawrence (2012). In most LSMs including CLASSIC, SND is diagnostically computed through snow water equivalent (W in Eq. (1)-(4)) and snow density (ρ_s): SND=W/ρ_s. Swenson and Lawrence (2012, their Fig. 7) illustrated that the rate of SCF increase with SND depends on the k_{acc} parameter, such that a larger k_{acc} parameter would result in faster SCF increase with SND. The default value from Swenson and Lawrence 2012) is 0.1 mm^{-1}, which is also used in our study. The impact of this choice will be discussed in Section 5.2.

During snowmelt:

$$f_{sno} = 1 - \left[\frac{1}{\pi}\text{acos}\left(2\frac{W}{W_{max}} - 1\right)\right]^{N_{melt}} \quad (2)$$

$$N_{melt} = \frac{200}{max(10,\ \sigma_{topo})} \quad (3)$$

$$W_{max} = \frac{W}{0.5\left(cos\left(\pi(1-f_{sno})^{\frac{1}{N_{melt}}}\right)+1\right)} \quad (4)$$

where the W and W_{max} are the current and the maximum accumulated snow water equivalent (mm), and N_{melt} (unitless) is a parameter determined from the standard deviation of topography, σ_{topo} (m). Eq. (4) is used to reconcile the relationship during periods of mixed accumulation and melt. Eq. (2) and Eq. (3) suggest that the rate of SCF decrease with SND depends on the N_{melt} parameter, such that SCF decreases faster with (normalized) SND in mountainous areas (small N_{melt}) than flat areas (large N_{melt}, Fig.9 in Swenson and Lawrence, 2012).

In our implementation we do not distinguish the use of these two formulations by time of year but based on whether SWE is increasing or decreasing with respect to the previous time step (Wang et al., 2025). To avoid the numerical instability issues mentioned above (Section 2.2.1), the SL12 parameterization is only used when the local SND over the snow-covered portion of a grid cell is greater than 0.1 m. When SND < 0.1 m, SCF is computed in the same way as in the default parameterization. Therefore, the largest difference in SCF between the default and SL12

https://doi.org/10.5194/egusphere-2025-1264
Preprint. Discussion started: 28 March 2025

parameterization as implemented in CLASSIC is expected in mountainous areas during the melt period. In these regions and times the topographic effects of sub-grid terrain is accounted for in SL12 but not in CTL.

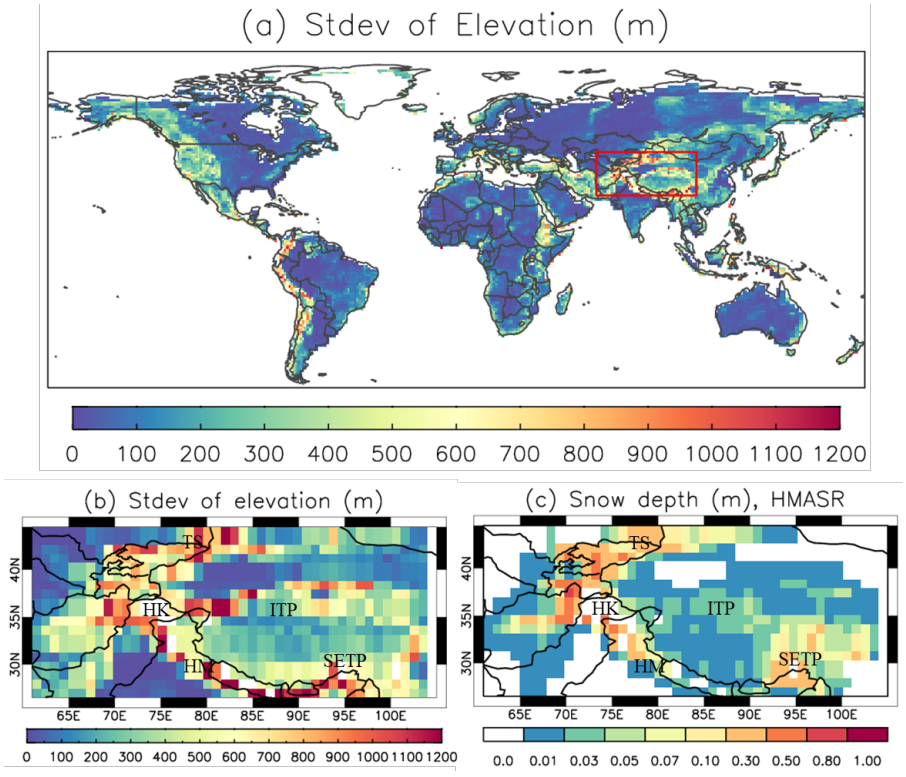

Figure1. (a) The standard deviation of elevation over the whole model domain; (b) the standard deviation of elevation in the HMA region (red rectangle box in (a)); (c) HMA mean snow depth during the main snow season (Sep – May) over the 2005-2014 period. Labels in (b) and (c) represent: Tibetan Plateau (TP), interior TP (ITP), southeastern TP (SETP), Tian Shan (TS), Hindu Kush–Karakoram (HK), and western Himalayas (HM).

2.3 Forcing data and simulation setup

The modeling domain chosen for this study is a global land only latitude-longitude grid at 1º resolution (Fig. 1a). Three gridded meteorological datasets are used to drive CLASSIC in this study: CRUJRA, ERA5, and GSWP3-W5E5, described below. CRUJRA is regularly used to drive LSMs participating the annual Global Carbon Project which provides analysis of the land carbon sink (Friedlingstein et al., 2025). It was constructed by regridding data from the Japanese reanalysis (JRA, Kobayashi et al., 2015) and adjusting where possible to align with the Climatic Research Unit (CRU) TS4 data (Harris, 2020; 2023). The blended product spanning January

https://doi.org/10.5194/egusphere-2025-1264
Preprint. Discussion started: 28 March 2025

1901 to December 2020 has the 6-hourly temporal resolution of the JRA reanalysis product but monthly means adjusted to match the CRU data at 0.5º spatial resolution.

ERA5 is the fifth generation European Centre for Medium-Range Weather Forecasts atmospheric reanalysis of the global climate covering the period from January 1940 to present (Hersbach et al., 2020). ERA5 data are available at hourly temporal and 0.25º spatial resolution. Currently it has the highest spatial and temporal resolutions available among all global reanalysis products.

GSWP3-W5E5 (here after referred as GSWP3W5) is a combination of two datasets: GSWP3 v1.09 (Dirmeyer et al., 2006; Kim 2017) from 1901-1978 and W5E5 v2.0 (Cucchi et al. 2020; Lange et al. 2021) from 1979-2019. It is one of the forcings used in the Inter-Sectoral Impact Model Intercomparison Project (ISIMIP). The GSWP3 dataset is a dynamically downscaled version of the Twentieth Century Reanalysis version 2 (20CRv2; Compo et al. 2011), bias-corrected using three separate observational data sets (see Kim 2017 for details). The W5E5 dataset is an interpolated version of ERA5 reanalysis, bias-corrected using CRU TS4. W5E5 also provides a second set of precipitation forcing data, bias-corrected with observations from the Global Precipitation Climatology Project (GPCP; Adler et al., 2003). The GPCP dataset includes around 3–4 times as many precipitation stations as CRU, thus we use this version of the precipitation forcing in our experiments. The GSWP3W5 data are available at daily temporal and 0.5º spatial resolution.

The three meteorological forcing datasets are regridded using the first order conservative remapping method to the 1º model grid via Climate Data Operators. They are disaggregated on the fly within CLASSIC into half-hourly data following the methodology of Melton and Arora (2016) for the following seven meteorological variables that are used to force the model: 2 m air temperature, total precipitation, specific humidity, downward solar radiation flux, downward longwave radiation flux, surface pressure, and wind speed. In CLASSIC, the phase of precipitation is determined by a threshold surface air temperature according to three possible options described in (Bartlett et al., 2006). Jennings et al. (2018) showed that the snowfall-rainfall transition temperature varied from -0.4°C to 2.4°C across the NH. Based on this, we used the option where the partitioning between rainfall and snowfall varies linearly between all rainfall at temperatures above 2º C, and all snowfall at temperatures below 0°C.

The plant functional types used in CLASSIC are derived from the Climate Change Initiative land cover product produced by the European Space Agency (Wang et al., 2023). The atmospheric CO_2 concentration values are provided by the Global Carbon Project (Le Quere et al., 2018). The soil texture information consists of the percentage of sand, clay, and organic matter and is derived from the SoilGrids250m dataset (Hengl et al., 2017), and the permeable soil depth is based on Shangguan et al. (2017).

CLASSIC simulations use either the CTL or the SL12 parameterization forced by the CRUJRA, ERA5, and GSWP3W5 respectively, yielding six simulations over the historical period. We refer to these simulations hereafter as: CRUJRA-CTL, CRUJRA-SL12, ERA5-CTL, ERA5-SL12, GSWP3W5-CTL, and GSWP3W5-SL12. Pre-industrial spin-up simulations were performed to allow the model to equilibrate carbon fluxes to conditions corresponding to the first year of the

https://doi.org/10.5194/egusphere-2025-1264
Preprint. Discussion started: 28 March 2025

forcing data. During spin-up, we loop climate data from the earliest 25 years available for CRUJRA/ERA5 and 100 years of spin-up data for GSWP3W5 (Lange et al., 2022), and hold atmospheric CO2 concentrations at the pre-industrial level (286.46 ppm). The transient runs use time-varying CO2 concentrations and climate. The period from 2005 to 2014 is selected for analyzing the simulated results, when there is overlap with the three observational SCF datasets (see Section 3.1).

3. Observation data and evaluation methods

3.1 Study area and evaluation methods

Our analysis will include evaluation of SCF, SWE, meteorological forcings, and other land surface variables. Assessment of SCF, SWE, and meteorological forcings will focus on the mountain (σ_{topo} > 200 m) and flat (σ_{topo} <= 200 m) regions over the Northern Hemisphere (NH), and sub-regions of North America (NA), Eurasia (EA), and HMA. Classification of mountain and flat regions is based on standard deviation of the sub-grid terrain from the ETOPO1 elevation data at 1 arc-minute resolution (NOAA, 2009). In the SL12 parameterization, the topographic effects of sub-grid terrain are considered via a Nmelt parameter (Eq. (2)), which is inversely related to σ_{topo} (Eq. (3)). Figure 1a shows that at 1º resolution, the magnitudes of σ_{topo} are around 200 m – 600 m for most of the mountainous regions except for the HMA and the Andes where the magnitude of σ_{topo} can reach 1200 m or more.

The HMA region is one of the most complex topographic areas on Earth, with very high sub-grid scale variability (Fig. 1b). It surrounds the Tibetan Plateau (TP), with an average elevation of 4000 m (Du and Qingsong, 2000). Considering the large SCF biases found in CanESM5 and other CMIP models in this region (e.g. Lalande et al., 2021), we will present results for HMA separately. Different regions of HMA exhibit different spatiotemporal patterns in snowfall and SWE due to its unique topography (Yao et al., 2012; Bolch et al., 2019). According to the High Mountainous Asia Snow Reanalysis (HMASR) dataset (see Section 3.2), during Sep. to May over 2005 to 2014 period, SND is only a few centimeters over most of the interior TP, with relatively deeper snow in southeastern TP (Fig. 1c). Deeper snow (SND > 0.2 m) is concentrated at the high elevations of the mountains where σ_{topo} is usually greater than 500 m, such as Tian Shan, Hindu Kush–Karakoram, and western Himalayas (Fig. 1c).

Gridded data are regridded using the first order conservative remapping method to the 1º latitude-longitude grid. In addition to the SCF and SWE data detailed below, the monthly air temperature and precipitation from CRU TS4 (Harris et al., 2020) are used as references to compare with the three meteorological forcing datasets. Evaluation metrics for SCF, SWE and meteorological forcing include the mean bias, unbiased root mean squared error (uRMSE) and Pearson correlation. The uRMSE is defined as the square root of the mean square error minus the squared bias: uRMSE = sqrt ($RMSE^2$ - $Bias^2$). Evaluation of other land surface variables is according to AMBER and detailed in Section 3.4.

https://doi.org/10.5194/egusphere-2025-1264
Preprint. Discussion started: 28 March 2025

3.2 SCF observations

The monthly SCF was obtained from the Moderate Resolution Imaging Spectroradiometer (MODIS) /Terra snow cover monthly L3 0.05º Climate Modeling Grid product (MOD10CM, version 61). This dataset provides monthly mean SCF based on the clearest views of the surface from 28 – 31 days of MOD10C1 daily observations and are available from the National Snow and Ice Data Center (Hall and Riggs, 2021). To mitigate the uncertainties in the MODIS product due to frequent cloud cover or complex terrains, SCF from the Interactive Multisensor Snow and Ice Mapping System (IMS) produced by the U.S. National Ice Center (2008) was also used as a reference in our analysis. The IMS dataset consists of binary snow/no snow information on a 4 km resolution polar stereographic projection grid (Helfrich et al. 2007). Though the binary format of this dataset is not ideal for SCF estimation, especially in areas around the snow line, SCF estimates from IMS are included because the resolution of our model is coarse (1º) and IMS data has been used to evaluate modelled SCF in previous studies (e.g. Wang et al., 2014; Orsolini et al., 2019). Daily IMS data were converted to monthly snow cover duration fraction (SCF = total number of days with snow cover in a month divided by the number of days in the month).

Previous studies suggested that there were large uncertainties in the SCF data from MODIS and IMS datasets in the HMA region (Hao et al., 2019; Orsolini et al., 2019). Thus the daily SCF from the HMASR dataset (Liu et al., 2021a) is used as an additional reference for the HMA region in this study. HMASR is based on a Bayesian snow reanalysis framework with model-based snow estimates refined through the assimilation of high resolution SCF data from MODIS (500 m) and Landsat (30 m) sensors (Liu et al., 2021b). The framework also accounts for a priori uncertainties in meteorological forcings and utilizes an ensemble approach (Margulis et al, 2019). The dataset provides daily data of posterior snow estimates at ~500 m spatial resolution over the HMA region. Ensemble mean values of SCF and SND are used in this study. The method used for HMASR was best suited for seasonal snow characterization (Liu et al. (2021a), thus grid cells with semi-permanent snow and ice greater than 30% are masked out in our analysis. The monthly SCF data from MODIS, IMS, and HMASR over the 2005-2014 period are used to evaluate modelled SCF.

3.3 SWE measurements

As shown in Eq. (1) and Eq. (2) simulated SCF is calculated from SWE directly in the SL12 parameterization, and from SND in the CTL parameterization (Section 2.2.1). Therefore, to better understand the sources of bias in simulated SCF, we also evaluate simulated SWE using snow course and airborne gamma SWE observations from Mortimer and Vionnet (2024) covering 1980 – 2014 (Fig. 2). Both types of in situ SWE information have previously been used to evaluate gridded products (e.g. Cho et al. 2019; Mortimer et al. 2020; Mudryk et al. 2025) and details of these data are described elsewhere (Mortimer et al. 2024, Mortimer and Vionnet 2025). Briefly, snow courses generally consist of multiple snow depth and density measurements collected along a predefined transect several hundred meters to several kilometers in length averaged together to obtain a single SWE value for each transect on a given date (WMO, 2018).

https://doi.org/10.5194/egusphere-2025-1264
Preprint. Discussion started: 28 March 2025

Airborne gamma SWE estimates are calculated by differencing snow-free and snow-covered measurements of gamma radiation collected along a 15-20 km long flight line with a 300 m wide footprint after accounting for background soil moisture (Carroll, 2001). Spatial distribution and measurement frequency of the observations varies by measurement method and jurisdiction (e.g. Fig. 2 in Mortimer and Vionnet, 2025). These measurements are better able to capture the larger-scale average compared to single point observations and have been shown capable of discerning subtle differences in SWE products (Mortimer et al. 2022) and of ranking such products based on their relative performance (Mudryk et al. 2025).

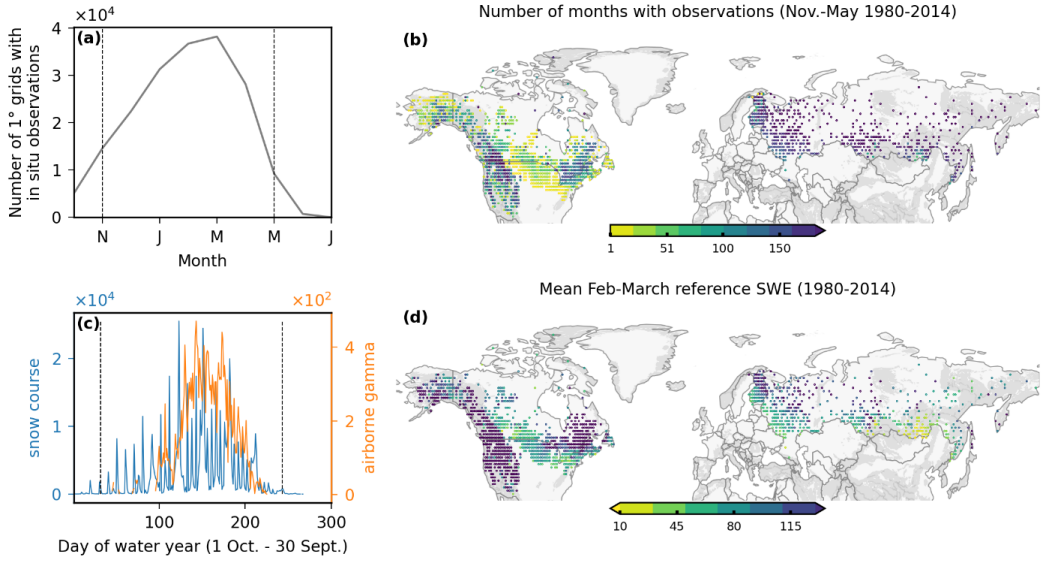

Figure 2. Distribution of in situ reference data. (a) Number of monthly 1°x1° grid cells with reference data during 1980-2014 (each monthly 1° grid with reference data is a data point), (b) Number of months during Nov-May 1980-2014 with reference observations by 1° grid. (c) Temporal distribution of raw in situ SWE observations. (d) Mean February-March reference SWE for grid cells with at least 5 months of data. Vertical lines in (a) and (c) indicate Nov-May period used in the analysis.

To evaluate monthly model output with reference observations from a specific date, we first match reference SWE observations to the model grid estimate from the corresponding month. Next, from these matched data, we calculate the mean reference SWE for each month. If there were multiple reference SWE observations within the same product grid cell on the same date, they were averaged prior to calculating the monthly mean. Metrics were calculated separately for mountainous and flat regions (see definition below) for each month (all years pooled together), for each year (all months pooled together), and for the full time period (all years and months pooled together), and for each product grid (all years pooled together). The analysis is limited to non-zero values with SWE < 3000 mm in both the observation and model outputs, and to the months November through May.

https://doi.org/10.5194/egusphere-2025-1264
Preprint. Discussion started: 28 March 2025

3.4 Reference datasets used to evaluate land surface variables in AMBER

Spatial and temporal variations of snow cover account for most of the variations in surface albedo due to its much higher reflectivity relative to underlying land surfaces. Changes in SCF thereby lead to changes in surface albedo, which in turn lead to changes in surface radiation and energy fluxes. To illustrate the impact of the SL12 parameterization on the simulated radiation, energy fluxes, and the water cycle in CLASSIC, we computed skill scores using the AMBER package (Seiler et al., 2021) for the global 1° simulations. AMBER assesses model performance against a collection of observation-based reference datasets based on five scores: bias (S_{bias}), root-mean-square-error (S_{rmse}), phase (S_{phase}), interannual variability (S_{iav}), and spatial distribution (S_{dist}). An overall score ($S_{overall}$) is calculated by averaging the five scores. The scores are dimensionless and on a scale from 0 to 1 where a higher value implies better model performance. Lower values are, however, not necessarily a product of poor model performance as the scores are also affected by uncertainties in the forcing and the reference data. Further details regarding the AMBER package as well as the skill score equations are presented in Seiler et al. (2021) and Seiler (2019). Table 1 shows the 21 reference datasets used in AMBER in this study, which contain information about seven variables relevant to the radiation, energy, and water cycle including net surface radiation (RNS), net surface shortwave radiation (RSS), net surface longwave radiation (RLS), surface albedo (ALBS), latent heat flux (HFLS), sensible heat flux (HFSS), and runoff (MRRO). These datasets include monthly mean values and more details can be found in Seiler et al. (2021).

Table 1. Overview of the reference datasets used in AMBER, including the following variables: net surface radiation (RNS), net surface shortwave radiation (RSS), net surface longwave radiation (RLS), surface albedo (ALBS), latent heat flux (HFLS), sensible heat flux (HFSS), and runoff (MRRO).

Dataset	Variables	Method	Period	References
CERES	ALBS, RSS, RLS, RNS	Radiative transfer model	2000-2013	Kato et al. (2013)
CLASSr	RNS, HFLS, HFSS, MRRO	Blended product	2003-2009	Hobeichi et al. (2020)
FLUXCOM	RNS, HFLS, HFSS	Machine learning ensemble	1980-2013	Jung et al. (2019)
FLUXNET	RNS, HFLS, HFSS	eddy covariance (204)	1997–2014	Pastorello et al. (2017)
GEWEXSRB	ALBS, RSS, RLS, RNS	radiative transfer model	1984-2007	Stackhouse et al. (2011)
GRDC	MRRO	gauge records (50)	1980–2010	Dai and Trenberth (2002)
GRUN	MRRO	Reconstruction via machine learning	1902-2014	Ghiggi et al. (2019)
MODIS	ALBS	Bidirectional Reflectance Distribution function	2000-2014	Schaaf and Wang (2015)

4. Results

https://doi.org/10.5194/egusphere-2025-1264
Preprint. Discussion started: 28 March 2025

4.1 Comparison of air temperature and precipitation in meteorological datasets

To better understand biases in the simulated snow cover, we first compare air temperature and precipitation from the three meteorological datasets with respect to CRU over the NH and HMA during the 1980-2014 period (Fig 3). Because the CRUJRA data is already bias-corrected to CRU temperature and precipitation, it exhibits very small biases in both variables in all regions. By comparison, both ERA5 and GSWP3W5 are colder during most of the months in the NH (Fig. 3a). The magnitude of the cold bias is larger in the mountainous than in the flat regions and larger in GSWP3W5 than in ERA5. Likewise, both ERA5 and GSWP3W5 have more precipitation than CRUJRA over the whole snow season. This difference is especially

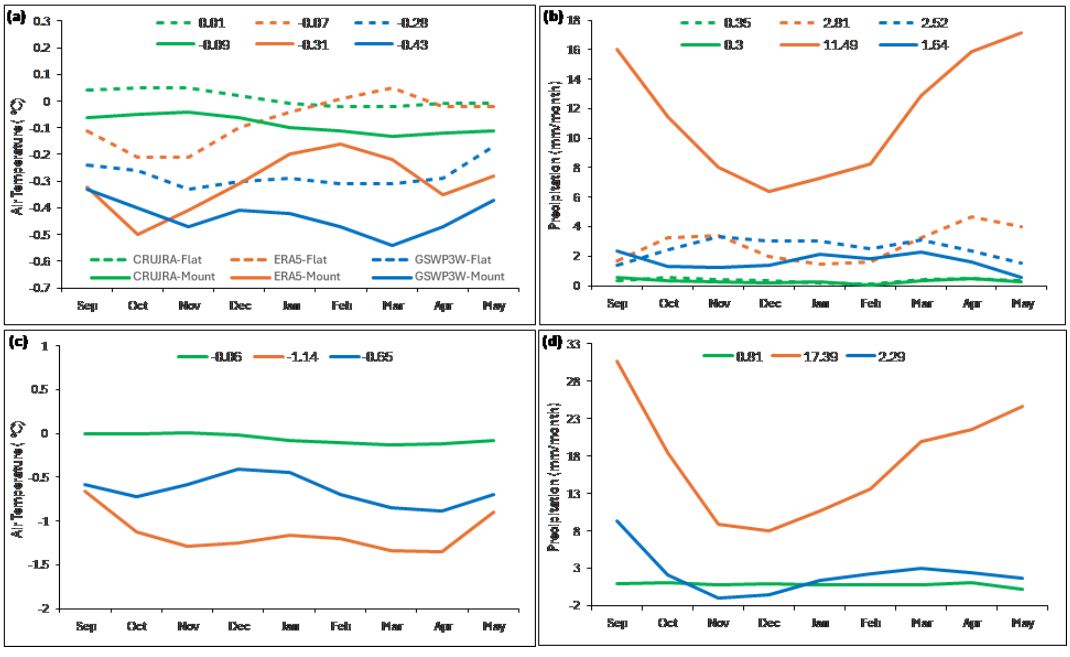

Figure 3. Bias in monthly mean air temperature (a and c) and precipitation (b and d) in the NH mountainous (solid line) and flat (dashed line) regions (a and b) and the HMA mountainous region (c and d) over the 1980-2014 period. Values shown at the top of each plot are the mean temperature or precipitation during Sep-May period for each dataset.

pronounced in ERA5 in the mountainous regions during the fall and spring months (Fig. 3b). In HMA, the bias patterns in temperature and precipitation are similar to those for mountainous regions across the full NH. However, the magnitude of the cold bias (with respect to CRU) is

https://doi.org/10.5194/egusphere-2025-1264
Preprint. Discussion started: 28 March 2025

larger in ERA5 than in GSWP3W5 (Fig. 3c). Because different reference datasets were used to bias-adjust precipitation in CRUJRA (CRU) and GSWP3W5 (GPCP), we also compare the monthly precipitation from CRU and GPCP in the above regions and over the same period. This analysis (not shown) indicates that the differences between CRU and GPCP are within 2 % and 3 % for NH flat and mountainous regions respectively, but up to 21 % in HMA.

4.2 Evaluation of SWE

Large difference in SWE from the model runs using the CTL and SL12 parameterizations are limited to small areas near grid cells with land ice because the runs are forced by the same three sets of meteorological datasets, and there is no feedback in offline runs. Thus we only present results for SWE from the model runs using the SL12 parameterization. The SWE reference measurements (Section 3.2) indicate that for all choices of meteorological forcing, CLASSIC underestimates SWE in mountainous regions (Fig. 4a) and overestimates SWE in flat regions (Fig. 4b) over the 1980-2014 period. For both types of regions, the magnitudes of the biases increase as the snow season progresses. In the mountainous regions, the biases are similar for

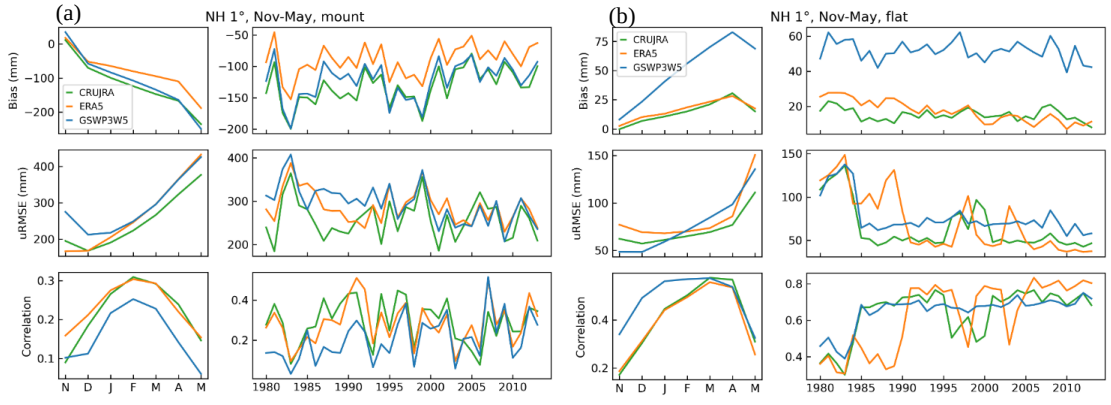

Figure 4. Annual and interannual evolution of bias, uRMSE, and correlation for modelled SWE in model runs using the SL12 parameterization forced by CRUJRA, ERA5, and GSWP3-W5E5 in (a) NH mountainous regions and (b) NH flat regions over the 1980-2014 period.

GSWP3W5 and CRUJRA and slightly smaller for ERA5. In flat regions, GSWP3W5-SL12 has more than twice the SWE bias seen in either CRUJRA-SL12 or ERA5-SL12, which is mainly due to SWE overestimation in eastern NA and northern Europe (Fig. A1). While in mountainous regions the uRMSE increases nearly linearly from Dec. to May, in flat regions, uRMSE remains under 100 mm from Nov to April but then increases sharply during April and May. Overall, ERA5-SL12 outperforms the other two model runs with lower bias and better correlation in mountainous regions and it shows similar performance as CRUJRA-SL12 in flat regions.

https://doi.org/10.5194/egusphere-2025-1264
Preprint. Discussion started: 28 March 2025

Table 2. The seasonal mean SCF bias, uRMSE, and Pearson correlation coefficient (r) for the Control and SL12 simulations over the (a) NH mountainous regions (σ_{topo} >200 m), (b) NH flat regions (σ_{topo} <= 200 m). The observed SCF from MODIS is used as the reference.

(a) NH Mountain	SON			DJF			MAM			Annual		
Met-Scheme	Bias	uRMSE	r	Bias	uRMSE	r	Bias	uRMSE	r	Bias	uRMSE	R
CRUJRA - CTL	-0.01	0.08	0.55	0.06	0.08	0.24	0.10	0.12	0.45	0.04	0.13	0.59
CRUJRA - SL12	-0.04	0.07	0.56	0.01	0.07	0.31	0.01	0.08	0.55	-0.01	0.09	0.62
ERA5 - CTL	0.01	0.06	0.59	0.07	0.07	0.28	0.09	0.11	0.48	0.05	0.12	0.62
ERA5 - SL12	-0.02	0.06	0.60	0.02	0.06	0.38	0.01	0.06	0.60	0.00	0.08	0.66
GSWP3W5 - CTL	-0.02	0.07	0.57	0.03	0.08	0.29	0.05	0.11	0.48	0.03	0.13	0.59
GSWP3W5-SL12	-0.04	0.07	0.58	-0.02	0.07	0.35	-0.03	0.07	0.56	-0.02	0.09	0.64
(b) NH Flat	SON			DJF			MAM			Annual		
Met-Scheme	Bias	uRMSE	r	Bias	uRMSE	r	Bias	uRMSE	r	Bias	uRMSE	r
CRUJRA - CTL	-0.02	0.07	0.57	0.02	0.05	0.20	0.09	0.12	0.44	0.03	0.11	0.59
CRUJRA - SL12	-0.04	0.08	0.57	0.01	0.06	0.24	0.08	0.11	0.47	0.02	0.11	0.59
ERA5 - CTL	-0.02	0.07	0.58	0.01	0.05	0.24	0.07	0.09	0.50	0.02	0.10	0.61
ERA5 - SL12	-0.04	0.08	0.58	0.00	0.05	0.27	0.06	0.09	0.52	0.01	0.10	0.61
GSWP3W5 - CTL	0.00	0.08	0.57	0.02	0.06	0.19	0.10	0.13	0.41	0.04	0.13	0.58
GSWP3W5-SL12	-0.02	0.08	0.57	0.01	0.06	0.23	0.09	0.13	0.45	0.03	0.12	0.58

4.3 Evaluation of SCF

4.3.1 NH regions

Figure 5 shows the monthly mean SCF (area weighted) from all six simulations along with the MODIS and IMS observations over different regions. SCF from MODIS and IMS generally agree well with each other in all regions except for HMA, where IMS shows ~3 % - 6 % more SCF than MODIS in the winter months (Fig. 5g). In the NH, NA, and EA mountainous regions (Fig. 5a-5c and Table 2), both the CTL and the SL12 parameterizations underestimate SCF in the fall (SON), with the SL12 parameterization performing slightly worse than the CTL parameterization. However, during winter (DJF) and spring (MAM), the SL12 parameterization greatly outperforms the CTL parameterization for all three meteorological datasets. For example, in the NH mountains during the spring, the mean biases are 0.1, 0.09, and 0.05 with the CTL parameterization for model runs forced by CRUJRA, ERA5, and GSWP3W5 respectively; they are 0.01, 0.01, and -0.03 with the SL12 parameterization (Table 2a). The uRMSEs are 0.12, 0.11, and 0.11 with the CTL parameterization, and 0.08, 0.06, and 0.07 with the SL12

https://doi.org/10.5194/egusphere-2025-1264
Preprint. Discussion started: 28 March 2025

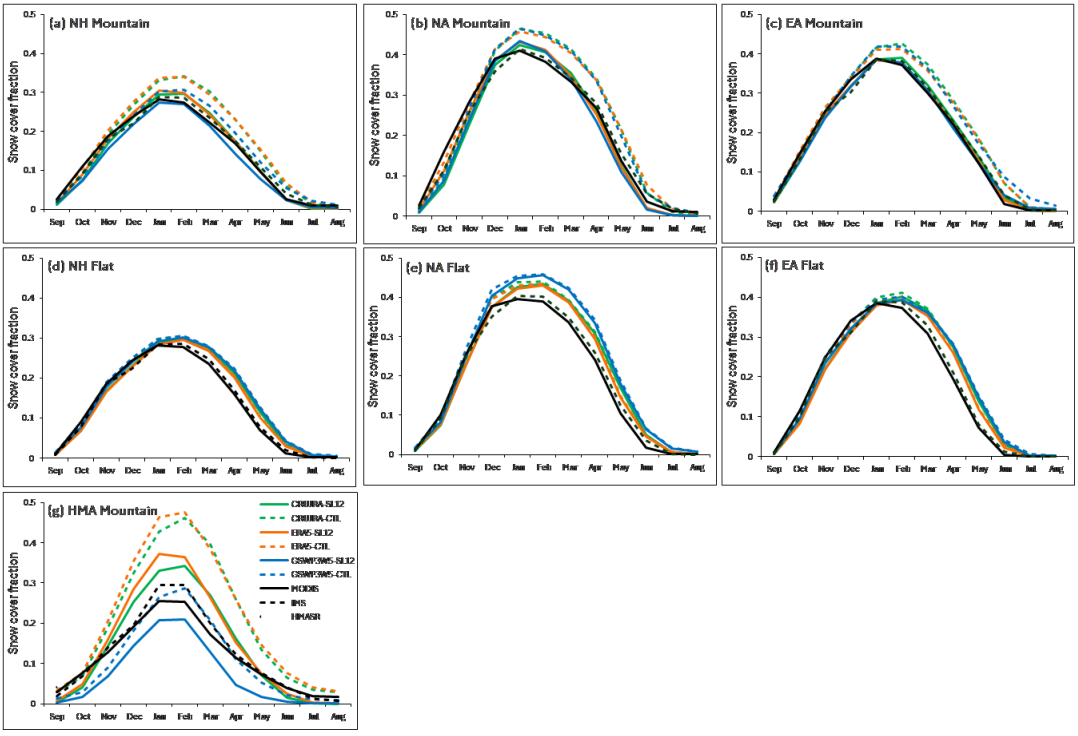

Figure 5. The monthly mean SCF from model runs using the Control (dashed line) and SL12 (solid line) parameterizations for NH, NA, and EA mountainous (σtopo $\geq$ 200 m, a-c) and flat (σtopo < 200 m, d-e) regions, and (g) shows the monthly mean SCF for the HMA mountainous region. The black lines represent observed SCF from MODIS (solid), IMS (dashed), and HMASR (dotted).

parameterization; and the correlation coefficients are 0.45, 0.48, and 0.48 with the CTL parameterization, and 0.55, 0.60, 0.56 with the SL12 parameterization (Table 2a). On average for all three meteorological forcing choices, the annual mean bias, uRMSE, and correlation improve by 75 %, 32 %, and 7 % when evaluated with MODIS SCF observations over the NH mountainous regions.

In flat regions (all domains), as expected, the performance is similar regardless of the parameterization with a 2-4 % SCF underestimation in the fall, but a 1-2 % and 6-10 % SCF overestimation during the winter and spring seasons, respectively (Fig. 5d-5f and Table 2b). Among the six simulations, ERA5-SL12 has the lowest annual bias (0.0) and uRMSE (0.08), and the highest correlation (0.66) in the NH mountainous regions, as well as in the flat regions (bias=0.01, uRMSE=0.1, and r=0.61) (Table 2).

https://doi.org/10.5194/egusphere-2025-1264
Preprint. Discussion started: 28 March 2025

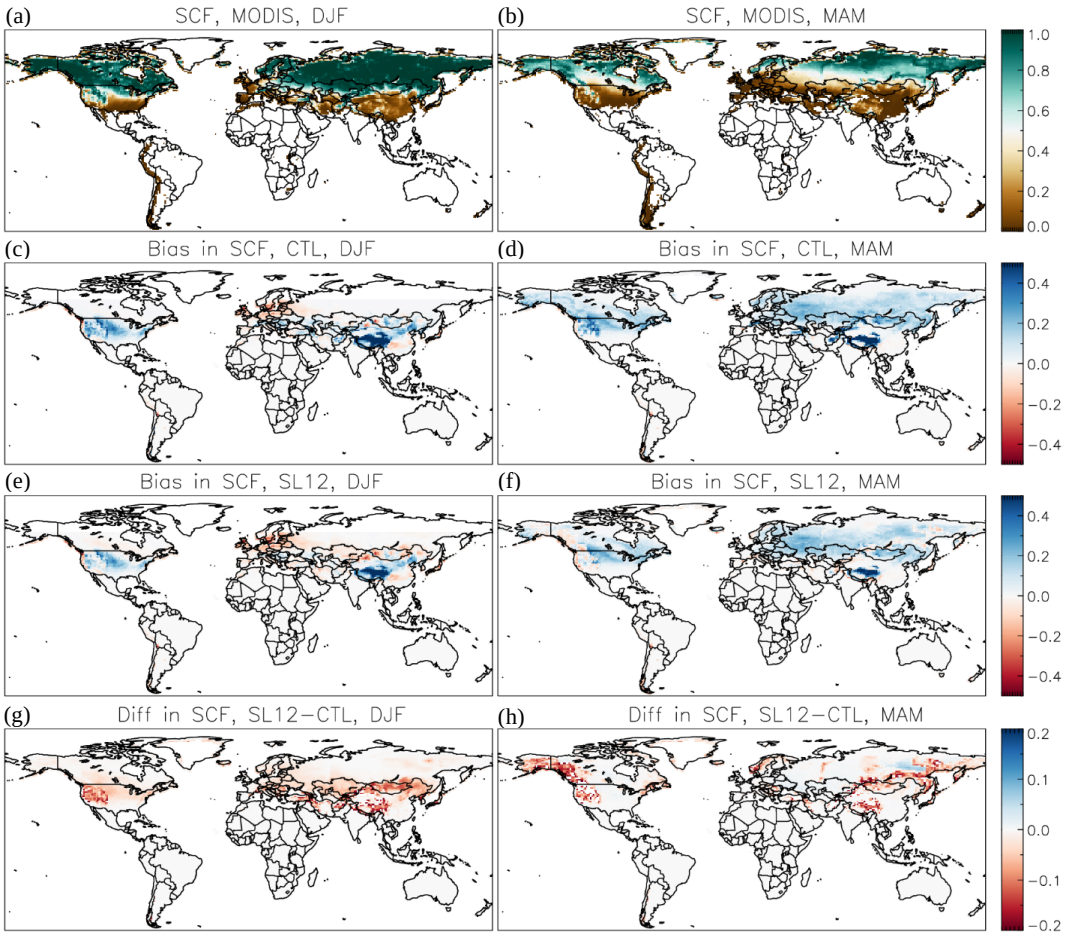

Figure 6. Snow cover fraction from MODIS (a and b), SCF bias in model runs using the Control (c and d) and SL12 (e and f) parameterizations, and difference in SCF between SL12 and Control (g and h) during the winter (left) and spring (right) season.

On the global scale, the spatial patterns of SCF bias are similar for all three meteorological forcing choices. Figure 6 shows an example of the spatial pattern in SCF bias from the model runs forced by ERA5 during the winter and spring seasons. Compared to observed SCF from MODIS, model runs tend to overestimate SCF in areas where SCF is less than 100 % in both the winter and spring seasons. In the winter, both parameterizations have areas with SCF underestimation, such as in the western NA mountainous areas, northern Europe, and some areas of Asia (Fig. 6c and 6e). In the spring, the CTL parameterization overestimates SCF in most NH regions except for some limited areas in western NA (Fig. 6d). The SCF overestimation is reduced in the run using the SL12 parameterization, and replaced with some SCF

https://doi.org/10.5194/egusphere-2025-1264
Preprint. Discussion started: 28 March 2025

underestimation, such as in the western NA mountains (Fig. 6f). Overall, the SL12 parameterization produces less SCF and thus reduces the SCF overestimation found in the model runs using the CTL parameterization over all major mountain ranges across the globe (Fig. 6g and 6h).

4.3.2 HMA region

In HMA, large uncertainties have been found in SCF from the MODIS and IMS datasets (Hao et al., 2019; Orsolini et al., 2019), thus SCF from the HMASR dataset is also included as a reference along with MODIS and IMS. Results are only shown for the mountainous region (Fig. 5g) because there are limited flat areas with snow cover (Fig. 1b and 1c). HMASR has a single peak in Feb., while MODIS, IMS, and all the model runs have peaks in both Jan. and Feb. Over this region, simulations using either parameterization exhibit large SCF overestimations during the winter and spring compared to all three reference datasets especially when forced by CRUJRA or ERA5 (Fig. 5g). Compared to SCF from HMASR, the mean biases are 0.30 and 0.35 in CRUJRA-CTL and ERA5-CTL respectively during the winter (Table 3). In contrast, the model runs driven by GSWP3W5 have much lower SCF and smaller biases (Fig. 5g and Table 3). Overall, the SL12 parameterization exhibits improved performance compared to the CTL parameterization. On average from all three meteorological forcing choices, the annual mean bias, uRMSE, and correlation improve by 48 %, 30 %, and 5 % when evaluated with HMASR SCF data over the HMA mountainous areas.

Table 3. Same as Table 2 but for the HMA region. SCF from the HMASR dataset is used as the reference.

HMA Mountain	SON			DJF			MAM			Annual		
Met-Scheme	Bias	uRMSE	r	Bias	uRMSE	r	Bias	uRMSE	r	Bias	uRMSE	r
CRUJRA - CTL	0.02	0.12	0.35	0.30	0.15	0.31	0.20	0.17	0.39	0.13	0.21	0.42
CRUJRA - SL12	-0.03	0.09	0.37	0.16	0.11	0.35	0.06	0.10	0.45	0.04	0.15	0.44
ERA5 - CTL	0.05	0.12	0.43	0.35	0.14	0.36	0.23	0.15	0.40	0.16	0.22	0.45
ERA5 - SL12	-0.01	0.09	0.45	0.22	0.11	0.42	0.08	0.09	0.51	0.06	0.15	0.48
GSWP3W - CTL	-0.06	0.08	0.40	0.08	0.14	0.39	0.01	0.12	0.44	0.00	0.14	0.45
GSWP3W - SL12	-0.08	0.07	0.41	0.00	0.11	0.39	-0.08	0.08	0.48	-0.05	0.10	0.46

In HMA, areas with high SCF (> 40 %) are mainly found along the western mountain ranges (e.g. Tian Shan, Hindu Kush–Karakoram, and western Himalayas) and southeast portion of the TP (Fig.7a-7c). SCF is less than 20 % in most of the interior TP, even during the winter (Fig. 7a). On average, maximum SCF occurs in winter in western HMA (i.e. Tian Shan and Hindu Kush–Karakoram), but it occurs in spring in interior TP and southeast TP. Among the model runs using the CTL parameterization, there are significant SCF overestimations in most of HMA when forced by CRUJRA or ERA5 (Fig. 7d, 7e). The run forced by GSWP3W5 still overestimates SCF in the mountainous areas of western HMA but underestimates SCF in the interior TP and southeast of TP (Fig. 7f). In the model runs using the SL12 parameterization (Fig. 7g-7i), the

https://doi.org/10.5194/egusphere-2025-1264
Preprint. Discussion started: 28 March 2025

SCF overestimations are much reduced in the western mountainous areas while across the rest of the plateau the SCF underestimations are very similar for both parameterizations.

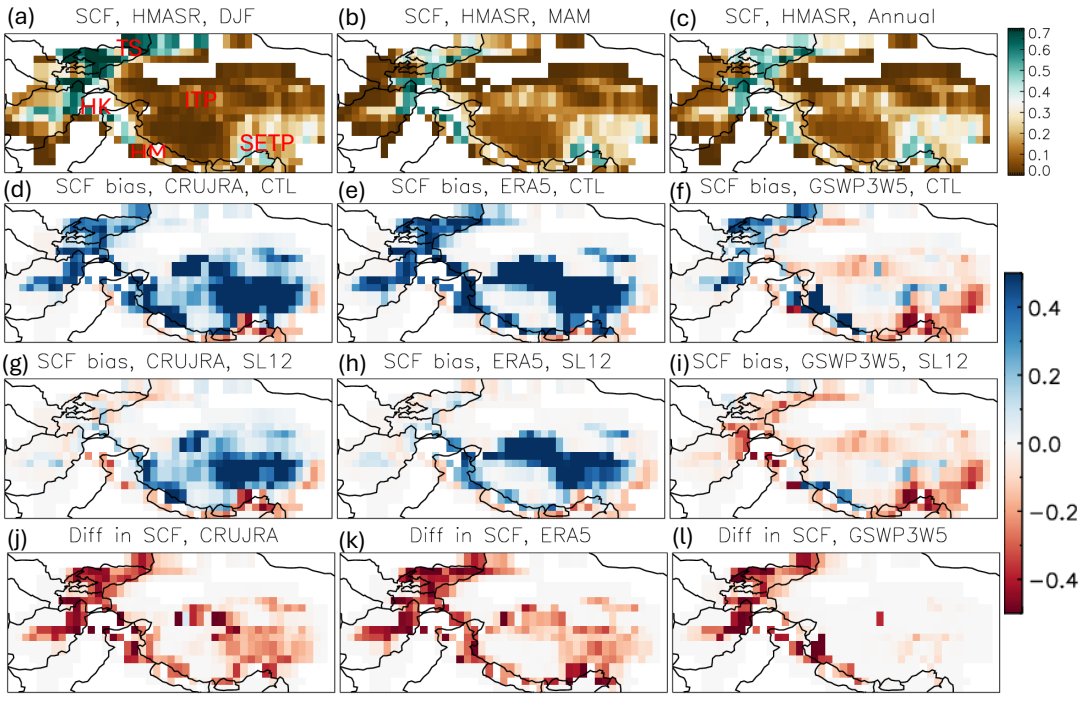

Figure 7. The top panel shows SCF from HMASR for (a) winter, (b) spring, and (c) annual mean. The second and third panel shows SCF biases from model runs using the CTL (d-f) and SL12 (g-i) parameterizations forced by the three meteorological datasets respectively during spring. The bottom panel (j-k) shows the difference in SCF between the model runs using the SL12 and CTL parameterizations.

4.4 Evaluation of other land surface variables

Evaluation of other land surface variables (besides SCF and SWE) via AMBER scores (Section 3.3) is shown in Fig. 8 for each of the six CLASSIC simulations. Model runs using the SL12 parameterization have the best score for 101 of 1119 diagnostic tests while they have the worst score for only 16 of 119 diagnostic tests (Fig. 8c and 8d). CRUJRA-SL12 (ID=2) and ERA5-SL12 (ID=4) have the highest overall scores for five radiation reference datasets (one RNS, two RSS, two RLS), and three surface albedo (ALBS) reference datasets with improvements ranging from 0.01 to 0.06 when compared to the runs with the lowest scores (Fig. 8b and 8c). The relatively large score differences in the interannual variability score (S_{iav}) for net surface radiation (RNS) suggests improved interannual variability of net surface radiation when using the SL12 parameterization (Fig. 8b). For surface albedo, the relatively large differences are in the

https://doi.org/10.5194/egusphere-2025-1264
Preprint. Discussion started: 28 March 2025

spatial distribution score (S_{dist}), suggesting better characterization of the spatial pattern in surface albedo when using the SL12 parameterization.

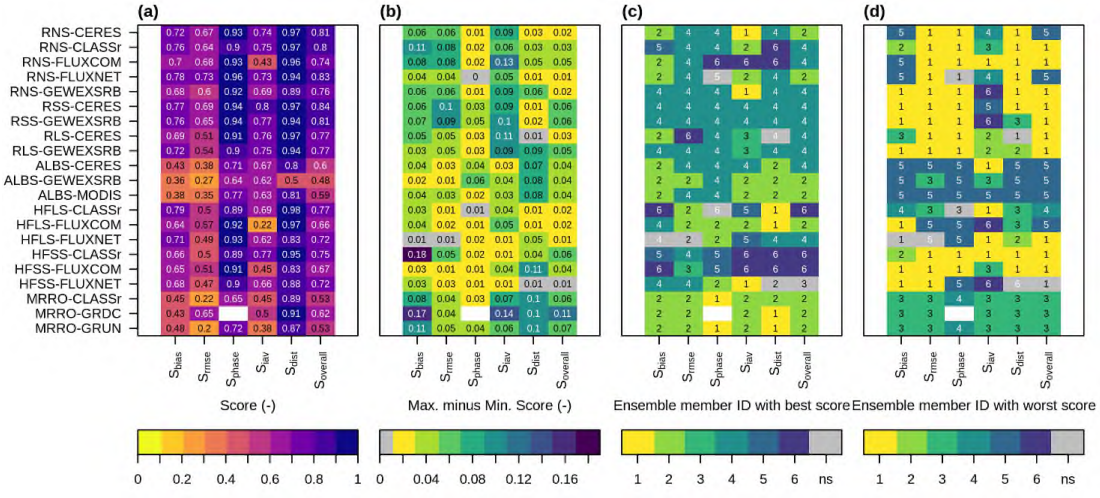

Figure 8. AMBER results for other land surface variables from the six model runs, (a) mean ensemble score, (b) maximum score difference among ensemble members, (c) ensemble member with the highest score, and (d) ensemble member with the lowest score. Comparisons are grayed out in panels (b–d) when the difference between the maximum and minimum scores is less than 0.01. Ensemble member IDs represent the following model runs: 1: CRUJRA-CTL, 2: CRUJRA-SL12, 3: ERA5-CTL, 4: ERA5-SL12, 5: GSWP3W5-CTL, 6: GSWP3W5-SL12.

Though GSWP3W5-SL12 (ID=6) has the lowest frequency of the model runs with the best scores (Fig. 8c), it has the highest overall performance for some of the heat fluxes datasets - one out of the three HFLS and two out of the three HFSS reference datasets. For surface runoff, model runs with the best scores are all forced by CRUJRA, while model runs with the worst scores are all forced by ERA5 (Fig. 8c and 8d).

To isolate the impact of meteorological forcing data and SCF parameterization on these snow-related variables, we also calculate AMBER scores for the three model runs separately for the SL12 (Fig. 9) and the CTL (Fig. A2) parameterizations. The results show that regardless of the parameterization, overall model runs forced by ERA5 (ID = 2) perform best for most radiation fluxes, while model runs forced by CRUJRA (ID = 1) perform best for the rest of the variables except for some heat fluxes where model runs forced by GSWP3W5 (ID = 3) perform best (Fig. 9c). These are generally consistent with results shown in Fig. 8 with both parameterizations included, suggesting that the score differences among ensemble members are largely due to differences in the meteorological forcing. However, the overall scores with the SL12 parameterization (Fig. 9a) are slightly larger for most variables than those with the CTL parameterization (Fig. A2a). Among the three model runs using the SL12 parameterization, ERA5-SL12 has the most (43/99) frequency in the model runs with the best scores (Fig. 9c), followed by CRUJRA-SL12 (38), with GSWP3W5-SL12 having the least frequency (18).

https://doi.org/10.5194/egusphere-2025-1264
Preprint. Discussion started: 28 March 2025

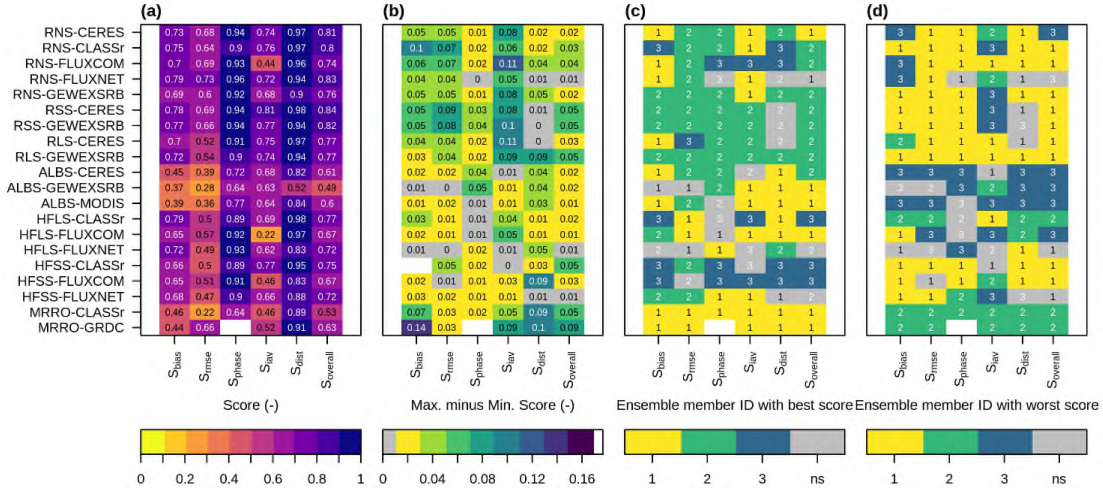

Figure 9. Same as in Fig. 8 except for the three model runs using the SL12 parameterization. Ensemble member IDs represent the following model runs: 1: CRUJRA-SL12, 2: ERA5-SL12, 3: GSWP3W5-SL12.

5. Discussion

This study evaluates the SL12 SCF parameterization against the current default (CTL) SCF parameterization on snow simulation in CLASSIC. To account for uncertainties in the forcing data, three reanalysis-based meteorological datasets are used to drive the model. Below we discuss the possible factors contributing to biases in the simulated SWE and SCF including potential biases in the meteorological forcing datasets.

5.1 Impacts of meteorological forcing datasets on modelled SWE

Evaluation based on measurements from snow course and airborne gamma data indicates that the magnitude of SWE bias and uRMSE seen in CLASSIC are comparable to those from other gridded SWE products and LSMs (Brown et al., 2018; Mortimer et al., 2024; Cho et al., 2022) intended to represent historical snow conditions. However, for all three choices of meteorological forcing SWE is underestimated in mountainous regions (Fig. 4a) and overestimated in flat regions (Fig. 4b) throughout the snow season (with subsequent impacts on SCF). Naively, the bias-adjustments applied to temperature and precipitation in both the CRUJRA and GSWP3W5 forcing data might be expected to result in more accurate simulations. Yet among the three choices of forcing we used, the unadjusted ERA5 data yielded the lowest bias when evaluating the simulated SWE in both mountainous and flat regions (Fig. 4, Fig. A1). In mountain regions, this discrepancy may result because the CRU and GPCP data used to adjust the precipitation values are biased towards locations with less precipitation (e.g. outside of regions with orographic features; e.g. Nijssen et al., 2001; Adler et al, 2003; Shi et al., 2017). Mountain precipitation underestimation was also linked to negative SWE biases based on

https://doi.org/10.5194/egusphere-2025-1264
Preprint. Discussion started: 28 March 2025

precipitation observations from the Snowpack Telemetry stations over western US (Cho et al. 2022).

In NH flat regions, precipitation values from CRU and GPCP are expected to be more accurate than in mountainous regions (Adler et al., 2003), so it is less clear why GSWP3W5 has a much larger SWE bias despite having a precipitation bias similar to ERA5. The fact that GSWP3W5 is colder in flat regions compared to the other two forcings could play a role (Fig. 3a). This may reduce its ability to simulate mid-season ablation events (e.g., Brown et al., 2006; Slater et al., 2001) and/or alter the timing and location of snowfall. The reason that GSWP3W5 is colder than CRUJRA is also not immediately clear since both products use CRU TS4 for bias-adjusting their temperature (see Section 2.3.2). Differences between the interpolation and bias-adjustment methods may be responsible for the differences since they are more complex for GSWP3W5 (see Cucchi et al., 2020 and Weedon et al., 2010) than CRUJRA (Harris, 2023). For example, a constant lapse rate of 6.5 K km^{-1} was applied to temperature correction in GSWP3W5 but not in CRUJRA.

These results highlight that there is uncertainty in the accuracy of both temperature and precipitation forcing even when bias-adjusted to observations. These uncertainties can propagate to uncertainty in simulated SWE directly through precipitation amounts or in the case of temperature through phase partitioning of rainfall versus snowfall or direct melt. Even with perfectly constrained bias-adjustments for temperature and precipitation individually, there may still be spread in simulated SWE stemming from uncertainties in the joint distribution of temperature and precipitation that determines when snowfall occurs. Although measurements from snow course and airborne gamma data used in this study can better sample the subgrid-scale variability than a single-point measurement, we acknowledge that there are still uncertainties in our evaluation results, e.g. in situ sites may be biased towards locations with more snow cover.

5.2 Factors contributing to residual bias in modelled SCF

Although SCF overestimation in the mountainous regions is much reduced by the SL12 parameterization compared to the CTL parameterization (Fig. 5a – 5c and 5g), there are still areas with notable SCF biases. For example, much of the western NA mountainous areas have negative biases during the spring with the SL12 parameterization (Fig. 6d and 6f). Furthermore, in flat areas, all model runs overestimate SCF (Fig. 5d – 5f). These remaining SCF biases may be at least partly attributable to SWE underestimation in mountainous regions and SWE overestimation in flat regions (Fig. 4). The fact that in flat regions, there are larger SWE biases (Fig. 4b) and correspondingly larger SCF overestimation (Fig. 5d – 5f) in the model runs forced by GSWP3W5 supports this argument (see Section 5.1). Below we present some evidence on the link between differences in meteorological forcing datasets and choices of parameter values in the SL12 parameterization and the bias in modelled SCF.

Overall NH performance for model runs driven by ERA5 is comparable or slightly better than the runs driven by CRUJRA in terms of simulated SWE and SCF (Fig. 3, Fig. 5, and Table 2), while model runs driven by GSWP3W5 are worse everywhere except for HMA. In HMA, there

https://doi.org/10.5194/egusphere-2025-1264
Preprint. Discussion started: 28 March 2025

is significant SCF overestimation in model runs forced by CRUJRA and ERA5, while model runs forced by GSWP3W5 have comparable SCF to observations (Fig. 5g and Table 3). For model runs forced by ERA5, this is consistent with the cold temperature bias and large precipitation overestimation in ERA5 (Fig. 3c and 3d). However, CRUJRA and GSWP3W5 exhibit similar biases in temperature and precipitation (Fig. 3c and 3d), yet model runs forced by them have contrasting SCF biases (Fig. 5g). Therefore, biases in temperature and precipitation cannot explain the SCF biases here. Instead, we found that the number of wet days (days with precipitation >= 0.1 mm) differs in each of the three datasets, especially in the HMA region (Fig. 10). Figure 10 shows that on average ERA5 has near-daily precipitation events in the mountainous areas (e.g. Tian Shan, Hindu Kush–Karakoram, and Himalayas) and southeast of TP, while GSWP3W5 has the fewest wet days over the whole HMA region, especially over the interior TP. The number of wet days in CRUJRA falls between the other two. This is consistent with differences in the SCF annual cycles (Fig. 5g) and the SCF bias patterns (Fig. 7) found among the three sets of model runs, suggesting that the different number of wet days in the forcings contributes most to the difference in modelled SCF in this region. This conclusion is also consistent with findings in previous studies (Liu et al., 2022; Orsolini et al., 2019), which suggested that excessive snowfall in ERA5 contributes to overestimation of SND, SWE, and SCF across HMA. In CLASSIC, the large number of wet days in ERA5 would lead to prolonged periods with fresh snow and therefore high snow albedo. In coupled simulations this could lead to or reinforce an existing cold bias. GSWP3W5 also has a smaller number of wet days in some other regions of the globe, such as the middle to high latitudes of NA and eastern Siberia (not shown).

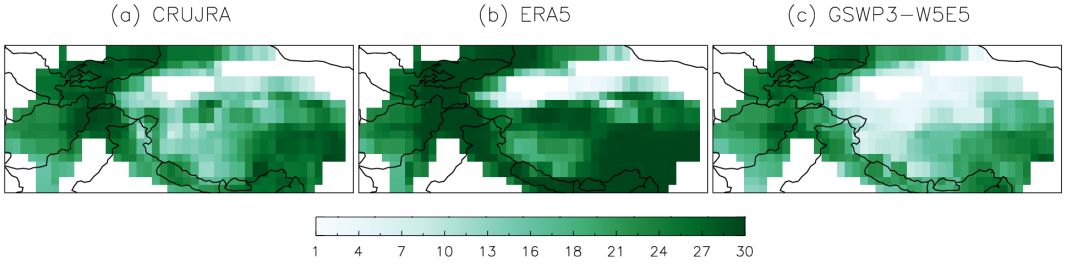

Figure 10. The monthly mean number of wet days (days with total Pr >= 0.1 mm) in (a) CRUJRA, (b) ERA5, and (c) GSWP3W5 during the main snow season (Sep – May) in HMA over the 2005-2014 period.

Besides biases in the meteorological datasets, the choice of parameter values in the SL12 parameterization can also contribute to uncertainties in modelled SCF. As illustrated in Swenson and Lawrence (2012, their Fig. 7), choosing a larger k_{acc} parameter in Eq. (1) would result in faster SCF increase with SND during accumulation events. All the previously discussed simulations have used the default value of 0.1 for this parameter. We also performed sensitivity experiments where the k_{acc} parameter was changed to 0.18 and 0.26. In these simulations, SCF increases faster with SND especially in the fall, thereby resulting in higher SCF over NH mountainous regions during that time of year. Notably, increasing k_{acc} to 0.26 produces less

https://doi.org/10.5194/egusphere-2025-1264
Preprint. Discussion started: 28 March 2025

biased SCF values during the fall (similar to those seen in the CTL simulations) while still maintaining the improvements already presented during winter and spring (Fig. A4).

Likewise, the ablation portion of the SL12 parameterization (Eq. (2)) can be altered via the N_{melt} parameter, which controls the rate at which SCF decreases as a function of SND. SCF decreases faster with (normalized) SND in mountainous areas (small N_{melt}) than flat areas (large N_{melt}, Fig. 9 in Swenson and Lawrence, 2012). We adjusted the N_{melt} parameter by increasing the numerator in Eq. (3) from 200 to 300, thereby increasing the N_{melt} value in mountain regions for the same value of sub-grid topographic variability and resulting in slower SCF decrease. Results of the test run show reduced SCF bias in the NA mountains in the spring compared to simulations with the default N_{melt} value (Fig. A5).

The adjustments to k_{acc} and N_{melt} parameters described above provide ways to fine-tune the agreement in simulated SCF with observations. However, because none of the three meteorological forcing datasets used in this study are exempt from biases, there is a limit to how well optimal parameter values can be chosen for use in CLASSIC.

6. Conclusions

Our results demonstrate that implementing the SL12 parameterization in CLASSIC improves simulated SCF in mountainous regions. This confirms that the lack of topographic dependency in the current default parameterization is at least partly responsible for the SCF overestimation and cold bias in the coupled model configuration, CanESM5 (Lalande et al., 2021; Swart et al. 2019; Sigmond et al., 2023). The improved simulation of SCF also improves the simulation of surface albedo, which in turn leads to improved simulation of the surface radiation, energy fluxes, and water cycle in CLASSIC.

The results also demonstrate that the choice of meteorological forcing data can have a large impact on snow simulation in offline LSM runs. Based on our analysis, we suggest that at least part of the SWE underestimation in mountainous areas and SWE overestimation in flat areas can be linked to relative biases in temperature and precipitation from the meteorological forcing datasets. The SWE biases then propagate to biases in modelled SCF. In addition, we highlighted that bias-adjustment methods that improve temperature or precipitation separately may not result in more accurately simulated SWE, with consequences for downstream components of the water and energy cycles related to snow. These meteorological forcing datasets are regularly used to drive LSMs in various projects, such as the Global Carbon Project and ISIMIP, but for snow simulations it is important to better understand how inaccuracies in temperature and precipitation can propagate to errors in modelled SWE and SCF.

Based on the evaluation results presented in this study along with preliminary test results in fully coupled CanESM runs, the SL12 parameterization has been adopted in CLASSIC and will be used in CanESM simulations for CMIP7 submission. Future work will focus on the evaluation of the SL12 parameterization in fully coupled CanESM simulations where a full analysis of feedbacks will be possible.

https://doi.org/10.5194/egusphere-2025-1264
Preprint. Discussion started: 28 March 2025

Code and data availability. The full CLASSIC code and resulting model outputs presented in this study are archived on Zenodo at: https://doi.org/10.5281/zenodo.15032447 (Wang et al., 2025).

Author contributions. LW conceived this research and LW and LM designed the study. LW, LM, JM, and CM developed the analysis framework. LW and PB implemented the SL12 parameterization into the CLASSIC code. LW conducted the analysis and wrote the first draft of the manuscript. All authors contributed to manuscript review and editing.

Competing interests. The contact author has declared that none of the authors has any competing interests.

Acknowledgements. We would like to thank Mike Brady (ECCC) and Ed Chan (ECCC) for their technical assistance.

References

Adler, R. F., Huffman, G. J., Chang, A., Ferraro, R., Xie, P., Janowiak, J., Rudolf, B., Schneider, U., Curtis, S., Bolvin, D., Gruber, A., Susskind, J., Arkin, P., & Nelkin, E.: The Version-2 Global Precipitation Climatology Project (GPCP) Monthly Precipitation Analysis (1979–Present), Journal of Hydrometeorology, 4(6), 1147-1167. https://doi.org/10.1175/1525-7541(2003)004%3C1147:TVGPCP%3E2.0.CO;2, 2003.

Arora, V. K. and Boer, G. J.: A parameterization of leaf phenology for the terrestrial ecosystem component of climate models, Glob. Chang. Biol., 11, 39–59, 2005.

AUER, A. H.: The rain versus snow threshold temperatures. Weatherwise, 27: 67, 1974.

Bartlett, P.A., MacKay, M. D., and Verseghy, D. L.: Modified snow algorithms in the Canadian Land Surface Scheme:Model runs and sensitivity analysis at three boreal forest stands. Atmos.–Ocean, 44, 207–222, doi:10.3137/ao.440301, 2006.

Betts, A. K., Viterbo, P., Beljaars, A., Pan, H. L., Hong, S. Y., Goulden, M., and Wofsy, S: Evaluation of land-surface interaction in ECMWF and NCEP/NCAR reanalysis models over grassland (FIFE) and boreal forest (BOREAS). J. Geophys. Res., 103 (D18), 23079–23085, doi:10.1029/98JD02023, 1998.

Bolch, T., Shea, J. M., Liu, S., Azam, F. M., Gao, Y., Gruber, S., Immerzeel, W. W., Kulkarni, A., Li, H., Tahir, A. A., Zhang, G., and Zhang, Y.: Status and Change of the Cryosphere in the Extended Hindu Kush Himalaya Region, in: The Hindu Kush Himalaya Assessment: Mountainous, Climate Change, Sustainability and People, edited by: Wester, P., Mishra, A., Mukherji, A., and Shrestha, A. B., Springer International Publishing, Cham, 209–255, 2019.

Brown, R., Brasnett, B., and Robinson, D: Gridded North American monthly snow depth and snow water equivalent for GCM evaluation. ATMOSPHERE-OCEAN, 41: 1–14, 2003.

https://doi.org/10.5194/egusphere-2025-1264
Preprint. Discussion started: 28 March 2025

Brown, R., Bartlett, P. A., MacKay, M., and Verseghy, D. L.: Evaluation of snow cover in CLASS for SnowMIP. Atmos.–Ocean, 44, 223–238, doi:10.3137/ao.440302, 2006.

Brown, R., Tapsoba, D., and Derksen, C.: Evaluation of snow water equivalent datasets over the Saint-Maurice river basin region of southern Québec, Hydrol. Process., 32, 2748–2764, 2018.

Carroll, T.R. Airborne Gamma Radiation Snow Survey Program: A user's guide, Version 5.0. National Operational Hydrologic Remote Sensing Center (NOHRSC), Chanhassen, 14, 2001.

Cho, E., Vuyovich, C. M., Kumar, S. V., Wrzesien, M. L., Kim, R. S., and Jacobs, J. M.: Precipitation biases and snow physics limitations drive the uncertainties in macroscale modeled snow water equivalent, Hydrol. Earth Syst. Sci., 26, 5721–5735, https://doi.org/10.5194/hess-26-5721-2022, 2022.

Clark, M. P., Hendrikx, J., Slater, A. G., Kavetski, D., Anderson, B., Cullen, N.J., Kerr, T., Hreinsson, E. O., and Woods, R. A.: Representing spatial variability of snow water equivalent in hydrologic and land-surface models: A review, Water Resour. Res., 47, W07539, doi:10.1029/2011WR010745, 2011.

Compo, G.P., Whitaker, J.S., Sardeshmukh, P.D., Matsui, N., Allan, R.J., Yin, X., Gleason, B.E., Vose, R.S., Rutledge, G., Bessemoulin, P., Brönnimann, S., Brunet, M., Crouthamel, R.I., Grant, A.N., Groisman, P.Y., Jones, P.D., Kruk, M.C., Kruger, A.C., Marshall, G.J., Maugeri, M., Mok, H.Y., Nordli, Ø., Ross, T.F., Trigo, R.M., Wang, X.L., Woodruff, S.D. and Worley, S.J.: The Twentieth Century Reanalysis Project. Q.J.R. Meteorol. Soc., 137: 1-28, https://doi.org/10.1002/qj.776, 2011

Cucchi, M., Weedon, G. P., Amici, A., Bellouin, N., Lange, S., Müller Schmied, H., Hersbach, H. and Buontempo, C.: WFDE5: bias-adjusted ERA5 reanalysis data for impact studies. Earth System Science Data, 12, 2097–2120, 2020.

Dai, A. and Trenberth, K. E.: Estimates of Freshwater Discharge from Continents: Latitudinal and Seasonal Variations, J. Hydrometeorol., 3, 660–687, 2002.

Dirmeyer, P. A., Gao, X., Zhao, M., Guo, Z., Oki, T. and Hanasaki, N.: GSWP-2: Multimodel Analysis and Implications for Our Perception of the Land Surface. Bulletin of the American Meteorological Society, 87(10), 1381–98, 2006.

Douville, H., Royer, J. F., and Mahfouf, J. F.: A new snow parameterization for the Météo-France climate model, Clim. Dynam.,12, 37–52, https://doi.org/10.1007/BF00208761, 1995.

Du, Z. and Qingsong, Z.: Introduction, in: Mountainous Geoecology and Sustainable Development of the Tibetan Plateau, Chap. 1, Springer, Dordrecht, 1–17, ISBN 978-94-010-3800-3, https://doi.org/10.1007/978-94-010-0965-2_1, 2000.

Elder, K., Dozier, J., and Michaelsen, J.: Snow accumulation and distribution in an alpine watershed, Water Resour. Res., 27, 1541–1552, doi:10.1029/91WR00506, 1991.

Eyring, V., Bony, S., Meehl, G. A., Senior, C. A., Stevens, B., Stouffer, R. J., & Taylor, K. E.: Overview of the Coupled Model Intercomparison Project Phase 6 (CMIP6) experimental design

and organization. Geoscientific Model Development, 9(5), 1937–1958. https://doi.org/10.5194/gmd-9-1937-2016, 2016.

Fletcher, C. G., Kushner, P. J., Hall, A., and Qu, X.: Circulation responses to snow albedo feedback in climate change. Geophys. Res. Lett., 36, L09702, doi:10.1029/2009GL038011, 2009.

Friedlingstein, P., O'Sullivan, M., Jones, M. W., Andrew, R. M., Hauck, J., Landschützer, P., Le Quéré, C., Li, H., Luijkx, I. T., Olsen, A., Peters, G. P., Peters, W., Pongratz, J., Schwingshackl, C., Sitch, S., Canadell, J. G., Ciais, P., Jackson, R. B., Alin, S. R., Arneth, A., Arora, V., Bates, N. R., Becker, M., Bellouin, N., Berghoff, C. F., Bittig, H. C., Bopp, L., Cadule, P., Campbell, K., Chamberlain, M. A., Chandra, N., Chevallier, F., Chini, L. P., Colligan, T., Decayeux, J., Djeutchouang, L. M., Dou, X., Duran Rojas, C., Enyo, K., Evans, W., Fay, A. R., Feely, R. A., Ford, D. J., Foster, A., Gasser, T., Gehlen, M., Gkritzalis, T., Grassi, G., Gregor, L., Gruber, N., Gürses, Ö., Harris, I., Hefner, M., Heinke, J., Hurtt, G. C., Iida, Y., Ilyina, T., Jacobson, A. R., Jain, A. K., Jarníková, T., Jersild, A., Jiang, F., Jin, Z., Kato, E., Keeling, R. F., Klein Goldewijk, K., Knauer, J., Korsbakken, J. I., Lan, X., Lauvset, S. K., Lefèvre, N., Liu, Z., Liu, J., Ma, L., Maksyutov, S., Marland, G., Mayot, N., McGuire, P. C., Metzl, N., Monacci, N. M., Morgan, E. J., Nakaoka, S.-I., Neill, C., Niwa, Y., Nützel, T., Olivier, L., Ono, T., Palmer, P. I., Pierrot, D., Qin, Z., Resplandy, L., Roobaert, A., Rosan, T. M., Rödenbeck, C., Schwinger, J., Smallman, T. L., Smith, S. M., Sospedra-Alfonso, R., Steinhoff, T., Sun, Q., Sutton, A. J., Séférian, R., Takao, S., Tatebe, H., Tian, H., Tilbrook, B., Torres, O., Tourigny, E., Tsujino, H., Tubiello, F., van der Werf, G., Wanninkhof, R., Wang, X., Yang, D., Yang, X., Yu, Z., Yuan, W., Yue, X., Zaehle, S., Zeng, N., and Zeng, J.: Global Carbon Budget 2024, Earth Syst. Sci. Data, 17, 965–1039, https://doi.org/10.5194/essd-17-965-2025, 2025.

Frolking, S., Milliman, T., McDonald, K., Kimball, J., Zhao, M., & Fahnestock, M.: Evaluation of the SeaWinds scatterometer for regional monitoring of vegetation phenology. Journal of Geophysical Research, 111, D17302. doi:10.1029/2005JD006588, 2006.

Ghiggi, G., Humphrey, V., Seneviratne, S. I., and Gudmundsson, L.: GRUN: an observation-based global gridded runoff dataset from 1902 to 2014, Earth Syst. Sci. Data, 11, 1655–1674, https://doi.org/10.5194/essd-11-1655-2019, 2019.

Hall, D. K. and Riggs, G. A.: MODIS/Terra Snow Cover Monthly L3 Global 0.05Deg CMG, Version 61. [Indicate subset used]. Boulder, Colorado USA. NASA National Snow and Ice Data Center Distributed Active Archive Center. https://doi.org/10.5067/MODIS/MOD10CM.061, 2021. [Last access September 2021].

Hao, S., Jiang, L., Shi, J., Wang, G., Liu, X.: Assessment of MODIS Based Fractional Snow Cover Products Over the Tibetan Plateau. IEEE J Sel Top Appl Earth Observations Remote Sens12:533–548, 2019.

Harris, I., Osborn, T. J., Jones, P., and Lister, D.: Version 4 of the CRU TS monthly high-resolution gridded multivariate climate dataset, Sci. Data, 7, 109, https://doi.org/10.1038/s41597-020-0453-3, 2020.

https://doi.org/10.5194/egusphere-2025-1264
Preprint. Discussion started: 28 March 2025

Harris, I.C.: CRU JRA v2.4: A forcings dataset of gridded land surface blend of Climatic Research Unit (CRU) and Japanese reanalysis (JRA) data; Jan.1901 - Dec.2022. NERC EDS Centre for Environmental Data Analysis, last access Sep. 2023. https://catalogue.ceda.ac.uk/uuid/aed8e269513f446fb1b5d2512bb387ad/, 2023.

Helfrich, S. R., D. McNamara, B. H. Ramsay, T. Baldwin, and T. Kasheta, 2007: Enhancements to, and forthcoming developments in the Interactive Multisensor Snow and Ice Mapping System (IMS). Hydrol. Processes, 21, 1576–1586, doi:10.1002/hyp.6720.

Hengl, T., Mendes de Jesus, J., Heuvelink, G. B. M., Ruiperez Gonzalez, M., Kilibarda, M., Blagoti´c, A., Shangguan, W., Wright, M. N., Geng, X., Bauer-Marschallinger, B., Guevara, M. A., Vargas, R., MacMillan, R. A., Batjes, N. H., Leenaars, J. G. B., Ribeiro, E., Wheeler, I., Mantel, S., and Kempen, B.: SoilGrids250m: Global gridded soil information based on machine learning, PLOS ONE, 12, 1–40, https://doi.org/10.1371/journal.pone.0169748, 2017

Hersbach, H., Bell, B., Berrisford, P., Hirahara, S., Horányi, A., Muñoz-Sabater, J., Nicolas, J., Peubey, C., Radu, R., Schepers, D., Simmons, A., Soci, C., Abdalla, S., Abellan, X., Balsamo, G., Bechtold, P., Biavati, G., Bidlot, J., Bonavita, M., Chiara, G., Dahlgren, P., Dee, D., Diamantakis, M., Dragani, R., Flemming, J., Forbes, R., Fuentes, M., Geer, A., Haimberger, L., Healy, S., Hogan, R. J., Hólm, E., Janisková, M., Keeley, S., Laloyaux, P., Lopez, P., Lupu, C., Radnoti, G., Rosnay, P., Rozum, I., Vamborg, F., Villaume, S., and Thépaut, J.-N.: The ERA5 global reanalysis, Q. J. Roy. Meteor. Soc., online first, https://doi.org/10.1002/qj.3803, 2020.

Hobeichi, S., Abramowitz, G. and Evans, J.: Conserving Land–Atmosphere Synthesis Suite (CLASS), Journal of climate, 33(5), pp. 1821–1844, 2020.

Jennings, K. S., Winchell, T. S., Livneh, B., & Molotch, N. P.: Spatial variation of the rain–snow temperature threshold across the Northern Hemisphere. Nature Communications, 9(1), 1–9. https://doi.org/10.1038/s41467-018-03629-7, 2018.

Jung, M., Koirala, S., Weber, U., Ichii, K., Gans, F., Camps-Valls, G., et al. : The FLUXCOM ensemble of global land-atmosphere energy fluxes. Scientific Data, 6(1), 74. https://doi.org/10.1038/s41597-019-0076-8, 2019.

Kato, S., Loeb, N. G., Rose, F. G., Doelling, D. R., Rutan, D. A., Caldwell, T. E., Yu, L., and Weller, R. A.: Surface Irradiances Consistent with CERES-Derived Top-of-Atmosphere Shortwave and Longwave Irradiances, J. Climate, 26, 2719–2740, 2013.

Kim, H.: Global Soil Wetness Project Phase 3 Atmospheric Boundary Conditions (Experiment 1) [Data set]. Data Integration and Analysis System (DIAS). https://doi.org/10.20783/DIAS.501, 2017.

Kobayashi, S., Ota, Y., Harada, Y., Ebita, A., Moriya, M., Onoda, H., Onogi, K., Kamahori, H., Kobayashi, C., Endo, H., Miyaoka, K., Takahashi, K.: The JRA-55 Reanalysis: General Specifications and Basic Characteristics. J. Met. Soc. Jap., 93(1), 5-48, https://dx.doi.org/10.2151/jmsj.2015-001, 2015.

https://doi.org/10.5194/egusphere-2025-1264
Preprint. Discussion started: 28 March 2025

Lalande, M., Ménégoz, M., Krinner, G., Naegeli, K., and Wunderle, S.: Climate change in the High Mountainous Asia in CMIP6, Earth System Dynamics, 12, 1061–1098, https://doi.org/10.5194/esd-12-1061-2021, 2021.

Lalande, M., Ménégoz, M., Krinner, G., Ottlé, C., and Cheruy, F.: Improving climate model skill over High Mountainous Asia by adapting snow cover parameterization to complex-topography areas, The Cryosphere, 17, 5095–5130, https://doi.org/10.5194/tc-17-5095-2023, 2023.

Lange, S.: Trend-preserving bias adjustment and statistical downscaling with ISIMIP3BASD (v1.0), Geosci. Model Dev., 12, 3055–3070, https://doi.org/10.5194/gmd-12-3055-2019, 2019.

Lange, S., Menz, C., Gleixner, S., Cucchi, M., Weedon, G.P., Amici, A., Bellouin, N., Müller-Schmied, H., Hersbach, H., Buontempo, C., Cagnazzo, C.: WFDE5 over land merged with ERA5 over the ocean (W5E5 v2.0), ISIMIP Repository, https://doi.org/10.48364/ISIMIP.342217, 2021.

Lange, S., Mengel, M., Treu, S., Büchner, M: ISIMIP3a atmospheric climate input data (v1.1), ISIMIP Repository, https://doi.org/10.48364/ISIMIP.982724.1, 2022.

Le Quéré, C., Andrew, R. M., Friedlingstein, P., Sitch, S., Hauck, J., Pongratz, J., Pickers, P. A., Korsbakken, J. I., Peters, G. P., Canadell, J. G., Arneth, A., Arora, V. K., Barbero, L., Bastos, A., Bopp, L., Chevallier, F., Chini, L. P., Ciais, P., Doney, S. C., Gkritzalis, T., Goll, D. S., Harris, I., Haverd, V., Hoffman, F. M., Hoppema, M., Houghton, R. A., Hurtt, G., Ilyina, T., Jain, A. K., Johannessen, T., Jones, C. D., Kato, E., Keeling, R. F., Goldewijk, K. K., Landschützer, P., Lefèvre, N., Lienert, S., Liu, Z., Lombardozzi, D., Metzl, N., Munro, D. R., Nabel, J. E. M. S., Nakaoka, S., Neill, C., Olsen, A., Ono, T., Patra, P., Peregon, A., Peters, W., Peylin, P., Pfeil, B., Pierrot, D., Poulter, B., Rehder, G., Resplandy, L., Robertson, E., Rocher, M., Rödenbeck, C., Schuster, U., Schwinger, J., Séférian, R., Skjelvan, I., Steinhoff, T., Sutton, A., Tans, P. P., Tian, H., Tilbrook, B., Tubiello, F. N., van der Laan-Luijkx, I. T., van der Werf, G. R., Viovy, N., Walker, A. P.,Wiltshire, A. J., Wright, R., Zaehle, S., and Zheng, B.: Global Carbon Budget 2018, Earth Syst. Sci. Data, 10, 2141–2194, https://doi.org/10.5194/essd-10-2141-2018, 2018.

Liston, G. E.: Representing subgrid snow cover heterogeneities in regional and global models. J. Climate, 17, 1381–1397, https://doi.org/10.1175/1520-0442(2004)017<1381:RSSCHI>2.0.CO;2, 2004.

Liu, Y., Fang, Y., and Margulis, S. A.: High Mountainous Asia UCLA Daily Snow Reanalysis, Version 1, Boulder, Colorado USA, NASA National Snow and Ice Data Center Distributed Active Archive Center [data set], https://doi.org/10.5067/HNAUGJQXSCVU, 2021a.

Liu, Y., Fang, Y., and Margulis, S. A.: Spatiotemporal distribution of seasonal snow water equivalent in High Mountainous Asia from an 18-year Landsat–MODIS era snow reanalysis dataset, The Cryosphere, 15, 5261–5280, https://doi.org/10.5194/tc-15-5261-2021, 2021b.

Liu, Y., Fang, Y., Li, D., and Margulis, S. A.: How well do global snow products characterize snow storage in High Mountainous Asia? Geophysical Research Letters, 49, e2022GL100082. https://doi.org/10.1029/2022GL100082, 2022.

https://doi.org/10.5194/egusphere-2025-1264
Preprint. Discussion started: 28 March 2025

Margulis, S. A., Liu, Y., and Baldo, E.: A Joint Landsat- and MODIS-Based Reanalysis Approach for Midlatitude Montane Seasonal Snow Characterization, Front. Earth Sci., 7, 1–23, https://doi.org/10.3389/feart.2019.00272, 2019.

Marshall, S. and Oglesby, R. J.: An improved snow hydrology for GCMs. Part 1: snow cover fraction, albedo, grain size, and age, Clim. Dynam., 10, 21–37, https://doi.org/10.1007/BF00210334, 1994.

Melton, J. R. and Arora, V. K.: Competition between plant functional types in the Canadian Terrestrial Ecosystem Model (CTEM) v. 2.0, Geosci. Model Dev., 9, 323–361, https://doi.org/10.5194/gmd-9-323-2016, 2016.

Melton, J. R., Verseghy, D. L., Sospedra-Alfonso, R., and Gruber, S.: Improving permafrost physics in the coupled Canadian Land Surface Scheme (v.3.6.2) and Canadian Terrestrial Ecosystem Model (v.2.1) (CLASS-CTEM), Geosci. Model Dev., 12, 4443–4467, https://doi.org/10.5194/gmd-12-4443-2019, 2019.

Melton, J. R., Arora, V. K., Wisernig-Cojoc, E., Seiler, C., Fortier, M., Chan, E., and Teckentrup, L.: CLASSIC v1.0: the open-source community successor to the Canadian Land Surface Scheme (CLASS) and the Canadian Terrestrial Ecosystem Model (CTEM) – Part 1: Model framework and site level performance, Geosci. Model Dev., 13, 2825–2850, https://doi.org/10.5194/gmd-13-2825-2020, 2020.

Miao, X., Guo, W., Qiu, B., Lu, S., Zhang, Y., Xue, Y., and Sun, S.: Accounting for Topographic Effects on Snow Cover Fraction and Surface Albedo Simulations Over the Tibetan Plateau in Winter, J. Adv. Model. Earth Sy., 14, e2022MS003035, https://doi.org/10.1029/2022MS003035, 2022.

Monteiro, D. and Morin, S.: Multi-decadal analysis of past winter temperature, precipitation and snow cover data in the European Alps from reanalyses, climate models and observational datasets, The Cryosphere, 17, 3617–3660, https://doi.org/10.5194/tc-17-3617-2023, 2023.

Myneni, R. B., Keeling, C. D., Tucker, C. J., Asrar, G., and Nemani, R. R.: Increased plant growth in the northern high latitudes from 1981 to 1991, Nature, 386, 698–702, doi:10.1038/386698a0, 1997.

Monteiro, D. and Morin, S.: Multi-decadal analysis of past winter temperature, precipitation and snow cover data in the European Alps from reanalyses, climate models and observational datasets, The Cryosphere, 17, 3617–3660, https://doi.org/10.5194/tc-17-3617-2023, 2023.

Mortimer, C., Mudryk, L., Derksen, C., Luojus, K., Brown, R., Kelly, R., and Tedesco, M.: Evaluation of long-term Northern Hemisphere snow water equivalent products, The Cryosphere, 14, 1579–1594, https://doi.org/10.5194/tc-14-1579-2020, 2020.

Mortimer, C., Mudryk, L., Derksen, C., Brady, M., Luo jus, K., Venäläinen, P., Moisander, M., Lemmetyinen, J., Takala, M., Tanis, C., and Pulliainen, J.: Benchmarking algorithm changes to the Snow CCI+ snow water equivalent product, Remote Sens. Environ., 274, 112988, https://doi.org/10.1016/j.rse.2022.112988, 2022.

https://doi.org/10.5194/egusphere-2025-1264
Preprint. Discussion started: 28 March 2025

Mortimer, C., and Vionnet, V.: Northern Hemisphere historical in-situ Snow Water Equivalent dataset (NorSWE, 1979-2021) (2.0) [data set]. Zenodo. https://doi.org/10.5281/zenodo.14503592, 2024.

Mortimer, C., Mudryk, L., Cho, E., Derksen, C., Brady, M., and Vuyovich, C.: Use of multiple reference data sources to cross-validate gridded snow water equivalent products over North America, The Cryosphere, 18, 5619–5639, https://doi.org/10.5194/tc-18-5619-2024, 2024.

Mortimer, C. and Vionnet, V.: Northern Hemisphere in situ snow water equivalent dataset (NorSWE, 1979–2021), Earth Syst. Sci. Data Discuss. [preprint], https://doi.org/10.5194/essd-2024-602, in review, 2025.

Mudryk, L., Mortimer, C., Derksen, C., Elias Chereque, A., and Kushner, P.: Benchmarking of snow water equivalent (SWE) products based on outcomes of the SnowPEx+ Intercomparison Project, The Cryosphere, 19, 201–218, https://doi.org/10.5194/tc-19-201-2025, 2025.

Namazi, M., von Salzen, K., and Cole, J. N. S.: Simulation of black carbon in snow and its climate impact in the Canadian Global Climate Model, Atmos. Chem. Phys., 15, 10887–10904, https://doi.org/10.5194/acp-15-10887-2015, 2015.

Nijssen, B., O'Donnell, G. M., Lettenmaier, D. P., Lohmann, D., and Wood, E. F.: Predicting the discharge of global rivers. J. Climate, 14, 3307–3323, 2001.

Niu, G.-Y. and Yang, Z.-L.: An observation-based formulation of snow cover fraction and its evaluation over large North American river basins, J. Geophys. Res., 112, D21101, https://doi.org/10.1029/2007JD008674, 2007.

NOAA National Geophysical Data Center: ETOPO1 1 Arc-Minute Global Relief Model, NOAA National Centers for Environmental Information, 2009. Accessed in Sep. 2021.

Orsolini, Y., Wegmann, M., Dutra, E., Liu, B., Balsamo, G., Yang, K., de Rosnay, P., Zhu, C., Wang, W., Senan, R., and Arduini, G.: Evaluation of snow depth and snow cover over the Tibetan Plateau in global reanalyses using in situ and satellite remote sensing observations, The Cryosphere, 13, 2221–2239, https://doi.org/10.5194/tc-13-2221-2019, 2019.

Osterkamp, T. E., & Romanovsky, V. E.: Evidence for warming and thawing of discontinuous permafrost in Alaska. Permafrost and Periglacial Processes, 10(1), 17−37, 1999.

Pastorello, G., Papale, D., Chu, H., Trotta, C., Agarwal, D., Canfora, E., Baldocchi, D., and Torn, M.: A new data set to keep a sharper eye on land-air exchanges, Eos T. Am. Geophys. Union, 98, https://doi.org/10.1029/2017EO071597, 2017.

Qu, X., and Hall, A.: On the persistent spread in snow-albedo feedback, Clim. Dyn., 42, 69–81, doi:10.1007/s00382-013-1774-0, 2013.

Roe, G. H., and Baker, M. B.: Why is climate sensitivity so unpredictable? Science, 318, 629–632, doi:10.1126/science.1144735, 2007.

https://doi.org/10.5194/egusphere-2025-1264
Preprint. Discussion started: 28 March 2025

Roesch, A., Wild, M., Gilgen, H., and Ohmura, A.: A new snow cover fraction parameterization for the ECHAM4 GCM, Clim. Dynam., 17, 933–946, https://doi.org/10.1007/s003820100153, 2001.

Schaaf, C., Wang, Z.: MCD43C3 MODIS/Terra+Aqua BRDF/Albedo Daily L3 0.05Deg CMG. NASA LP DAAC, http://doi.org/10.5067/MODIS/MCD43C3.006, 2015.

Seiler, C.: amber: Automated model benchmarking package for the Canadian land surface scheme, 2019.

Seiler, C., Melton, J. R., Arora, V. K., and Wang, L.: CLASSIC v1.0: the open-source community successor to the Canadian Land Surface Scheme (CLASS) and the Canadian Terrestrial Ecosystem Model (CTEM) – Part 2: Global Benchmarking, Geoscientific Model Development, https://doi.org/10.5194/gmd-14-2371-2021, 2021.

Shangguan, W., Hengl, T., Mendes de Jesus, J., Yuan, H., and Dai, Y.: Mapping the global depth to bedrock for land surface modeling, J. Adv. Model. Earth Syst., 9, 65–88, https://doi.org/10.1002/2016MS000686, 2017.

Shi, H., Li, T., Wei, J.: Evaluation of the gridded CRU TS precipitation dataset with the point raingauge records over the Three-River Headwaters Region, Journal of Hydrology, 548, 322-332, https://doi.org/10.1016/j.jhydrol.2017.03.017, 2017.

Sigmond, M., Anstey, J., Arora, V., Digby, R., Gillett, N., Kharin, V., Merryfield, W., Reader, C., Scinocca, J., Swart, N., Virgin, J., Abraham, C., Cole, J., Lambert, N., Lee, W.-S., Liang, Y., Malinina, E., Rieger, L., von Salzen, K., Seiler, C., Seinen, C., Shao, A., Sospedra-Alfonso, R., Wang, L., and Yang, D.: Improvements in the Canadian Earth System Model (CanESM) through systematic model analysis: CanESM5.0 and CanESM5.1, Geosci. Model Dev., 16, 6553–6591, https://doi.org/10.5194/gmd-16-6553-2023, 2023.

Slater, A. G., Schlosser, C. A., Desborough, C. E., Pitman, A. J., Henderson-Sellers, A., Robock, A., Vinnikov, K. Y., Entin, J., Mitchell, K., Chen, F., Boone, A., Etchevers, P., Habets, F., Noilhan, J., Braden, H., Cox, P. M., de Rosnay, P., Dickinson, R. E., Yang, Z.-L., Dai, Y.-J., Zeng, Q., Duan, Q., Koren, V., Schaake, S., Gedney, N., Gusev, Y. M., Nasonova, O. N., Kim, J., Kowalczyk, E. A., Shmakin, A. B., Smirnova, T. G., Verseghy, D.,Wetzel, P., and Xue, Y.: The representation of snow in land surface schemes: Results from PILPS 2(d), J. Hydrometeorol., 2, 7–25, 2001.

Lange, S., Menz, C., Gleixner, S., Cucchi, M., Weedon, G. P., Amici, A., Bellouin, N., Schmied, H. M., Hersbach, H., Buontempo, C., Cagnazzo, C.: WFDE5 over land merged with ERA5 over the ocean (W5E5 v2.0). ISIMIP Repository. https://doi.org/10.48364/ISIMIP.342217, 2021.

Stackhouse, Jr, P. W., Gupta, S. K., Cox, S. J., Zhang, T., Mikovitz, J. C., and Hinkelman, L. M.: The NASA/GEWEX surface radiation budget release 3.0: 24.5-year dataset, Gewex news, 21, 10–12, 2011.

Su, F., Duan, X., Chen, D., Hao, Z., and Cuo, L.: Evaluation of the Global Climate Models in the CMIP5 over the Tibetan Plateau, J. Climate, 26, 3187–3208, https://doi.org/10.1175/JCLI-D-12-00321.1, 2013.

https://doi.org/10.5194/egusphere-2025-1264
Preprint. Discussion started: 28 March 2025

Swart, N. C., Cole, J. N. S., Kharin, V. V., Lazare, M., Scinocca, J. F., Gillett, N. P., Anstey, J., Arora, V., Christian, J. R., Hanna, S., Jiao, Y., Lee, W. G., Majaess, F., Saenko, O. A., Seiler, C., Seinen, C., Shao, A., Sigmond, M., Solheim, L., von Salzen, K., Yang, D., and Winter, B.: The Canadian Earth System Model version 5 (CanESM5.0.3), Geosci. Model Dev., 12, 4823–4873, https://doi.org/10.5194/gmd-12-4823-2019, 2019.

Swenson, S. C. and Lawrence, D. M.: A new fractional snow-covered area parameterization for the Community Land Model and its effect on the surface energy balance, J. Geophys. Res.-Atmos., 117, D21107, https://doi.org/10.1029/2012JD018178, 2012.

Taylor, K. E., Stouffer, R. J., & Meehl, G. A.: An overview of CMIP5 and the experiment design. Bulletin of the American Meteorological Society, 93(4), 485–498, https://doi.org/10.1175/BAMS-D-11-00094.1, 2012.

U.S. National Ice Center: IMS Daily Northern Hemisphere Snow and Ice Analysis at 1 km, 4 km, and 24 km Resolutions. (G02156, Version 1). [Data Set]. Boulder, Colorado USA. National Snow and Ice Data Center. https://doi.org/10.7265/N52R3PMC, 2008. Date Accessed Oct. 22, 2024.

Verseghy, D. L.: CLASS – A Canadian Land Surface Scheme for GCMs, I. Soil model, Int. J. Climatol., 11, 111–133, https://doi.org/10.1002/joc.3370110202, 1991.

Verseghy, D., McFarlane, N., and Lazare, M.: Class – A Canadian land surface scheme for GCMs, II: Vegetation model and coupled runs, Int. J. Climatol., 13, 347–370, https://doi.org/10.1002/joc.3370130402, 1993.

Verseghy, D., Brown, R., & Wang, L.: Evaluation of CLASS Snow Simulation over Eastern Canada. Journal of Hydrometeorology, 18(5), 1205–1225. https://doi.org/10.1175/JHM-D-16-0153.1, 2017.

Wang, L., MacKay, M., Brown, R., Bartlett, P., Harvey, R., and Langlois, A: Application of satellite data for evaluating the cold climate performance of the Canadian Regional Climate model over Québec, Canada, Journal of Hydrometeorology, 15, 614-630, 2014.

Wang, L., Arora, V. K., Bartlett, P., Chan, E., and Curasi, S. R.: Mapping of ESA-CCI land cover data to plant functional types for use in the CLASSIC land model, Biogeosciences, 20, 2265–2282, https://doi.org/10.5194/bg-20-2265-2023, 2023.

Wang, L., Mudryk, L., Melton, J. R., Mortimer, C., Cole, J., Meyer, G., Bartlett, P., & Lalande, M.: Impact of topography and meteorological forcing on snow simulation in the Canadian Land Surface Scheme Including Biogeochemical Cycles (CLASSIC). https://doi.org/10.5281/zenodo.15032447, 2025.

Weedon, G. P., Gomes, S., Viterbo, P., Österle, H., Adam, J. C., Bellouin, N., Boucher, O., and Best, M.: The WATCH Forcing Data 1958–2001: A meteorological forcing dataset for land surface and hydrological-models, Tech. rep., WATCH Technical Report 22, available at: http://www.eu-watch.org/publications/technical-reports (last access: 26 August 2020), 2010.

https://doi.org/10.5194/egusphere-2025-1264
Preprint. Discussion started: 28 March 2025

Weedon, G. P., Balsamo, G., Bellouin, N., Gomes, S., Best, M. J., and Viterbo, P.: The WFDEI meteorological forcing data set: WATCH Forcing Data methodology applied to ERAInterim reanalysis data, Water Resour. Res., 50, 7505–7514, https://doi.org/10.1002/2014WR015638, 2014.

WMO (Ed.): Guide to instruments and methods of observation: Volume II - Measurement of Cryospheric Variables, 2018th ed., World Meteorological Organization, Geneva, WMO-No. 8, 52 pp., 2018.

Yang, Z.-L., Dickinson, R. E., Robock, A., and Vinnikov, K. Y.: Validation of the Snow Submodel of the Biosphere–Atmosphere Transfer Scheme with Russian Snow Cover and Meteorological Observational Data, J. Climate, 10, 353–373, https://doi.org/10.1175/1520-0442(1997)010<0353:VOTSSO>2.0.CO;2, 1997.

Yao, T., Thompson, L. G., Mosbrugger, V., Zhang, F., Ma, Y., Luo, T., Xu, B., Yang, X., Joswiak, D. R., Wang, W., Joswiak, M. E., Devkota, L. P., Tayal, S., Jilani, R., and Fayziev, R.: Third Pole Environment (TPE), Environmental Development, 3, 52–64, https://doi.org/10.1016/j.envdev.2012.04.002, 2012.

https://doi.org/10.5194/egusphere-2025-1264
Preprint. Discussion started: 28 March 2025

Appendix A:

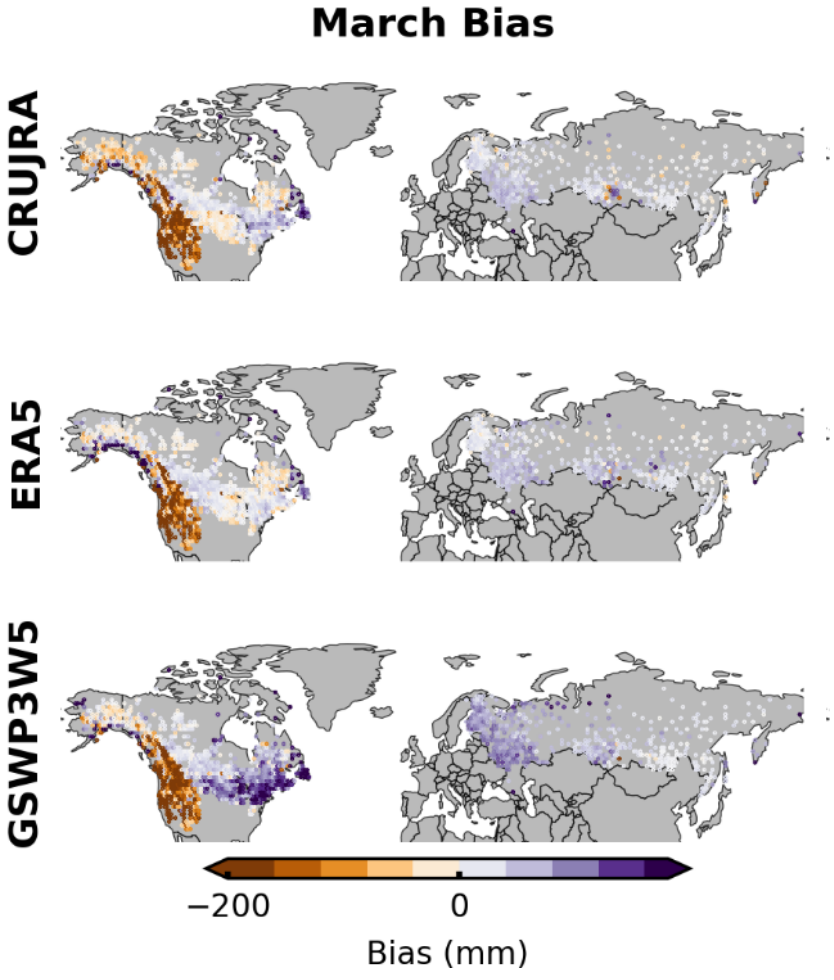

Figure A1. March SWE bias relative to in situ measurements over the 1980-2014 period from model runs forced by each of the three meteorological forcings.

https://doi.org/10.5194/egusphere-2025-1264
Preprint. Discussion started: 28 March 2025

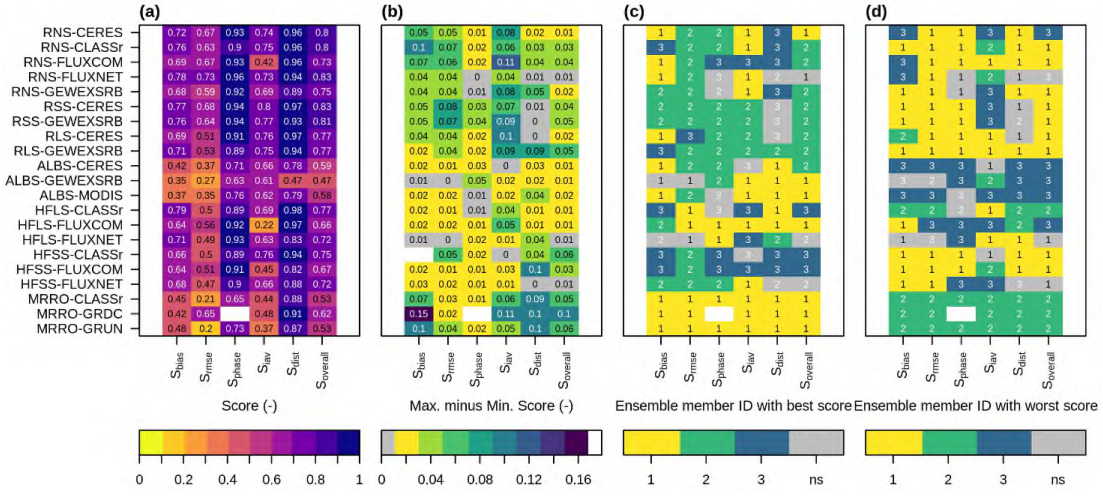

Figure A2. AMBER results for other land surface variables from three model runs using the CTL parameterization, (a) mean ensemble score, (b) maximum score difference among ensemble members, (c) ensemble member with the highest score, and (d) ensemble member with the lowest score. Ensemble member IDs represent the following model runs: 1: CRUJRA-CTL, 2: ERA5-CTL, 3: GSWP3W5-CTL.

https://doi.org/10.5194/egusphere-2025-1264
Preprint. Discussion started: 28 March 2025

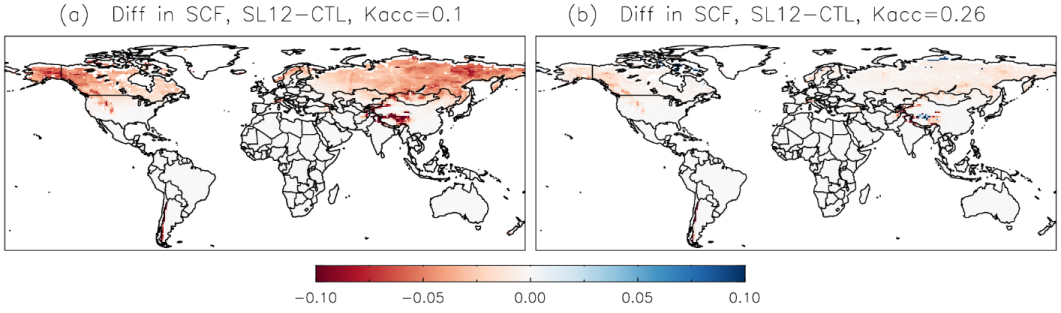

Figure A3. The difference in SCF between SL12 and Control parameterization during the fall in model runs using (a) k_{acc}=0.1, and (b) k_{acc}=0.26 for the SL12 parameterization.

https://doi.org/10.5194/egusphere-2025-1264
Preprint. Discussion started: 28 March 2025

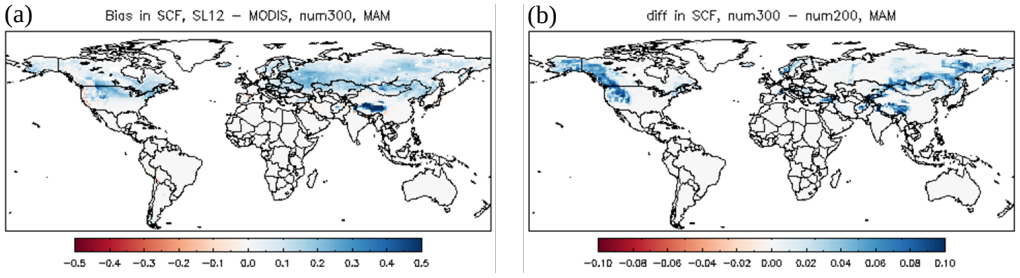

Figure A4. (a) Spring SCF bias relative to MODIS using adjusted N_{melt} parameter (numerator=300 in Eq. 3), and (b) difference in spring SCF in model runs using adjusted and default (numerator=200 in Eq. 3) N_{melt} parameter.